The water-insoluble organic carbon in PM$_{2.5}$ of typical Chinese urban areas: light-absorbing properties, potential sources, radiative forcing effects and possible light-absorbing continuum

Yangzhi Mo[1, 2], Jun Li [1, 2], Guangcai Zhong[1, 2], Sanyuan Zhu[1, 2], Shizhen Zhao[1, 2], Jiao Tang[1, 2], Hongxing Jiang[3], Zhineng Cheng[1, 2], Chongguo Tian[4], Yingjun Chen[3], Gan Zhang[*,1, 2]

[1] State Key Laboratory of Organic Geochemistry and Guangdong province Key Laboratory of Environmental Protection and Guangdong-Hong Kong-Macao Joint Laboratory for Environmental Pollution and Control, Guangzhou Institute of Geochemistry, Chinese Academy of Science, Guangzhou 510640, China

[2] CAS Center for Excellence in Deep Earth Science, Guangzhou, 510640, China

[3] Shanghai Key Laboratory of Atmospheric Particle Pollution and Prevention (LAP3), Department of Environmental Science and Engineering, Fudan University, Shanghai 200438, China

[4] Key Laboratory of Coastal Environmental Processes and Ecological Remediation, Yantai Institute of Coastal Zone Research, Chinese Academy of Sciences, Yantai, 264003, China

[*]Corresponding author: Dr. Gan Zhang

E-mail: zhanggan@gig.ac.cn; Tel: +86-20-85290805; Fax: +86-20-85290706;

Abstract

Water-insoluble organic carbon (WIOC) constitutes a substantial portion of organic carbon (OC) and contributes significantly to light absorption by brown carbon (BrC), playing pivotal roles in climate forcing. China as hotspots regions with high level of OC and BrC, information regarding the sources and light-absorbing properties of WIOC on national scale remains scarce. Here, we investigated the light-absorbing properties and sources of WIOC in ten representative urban cities in China. On average, WIOC made up 33.4 ± 7.66% and 40.5 ± 9.73% of concentrations and light absorption at 365 nm (Abs$_{365}$) of extractable OC (EX-OC), which includes relatively hydrophobic OC (WIOC and humic-like substances: HULIS-C) and hydrophilic OC (non-humic-like substances: non-HULIS-C). The mass absorption efficiency of WIOC

at 365 nm (MAE_{365}) was (1.59 ± 0.55 m^2/gC) comparable to that of HULIS (1.54 ± 0.57 m^2/gC) but significantly higher than non-HULIS (0.71 ± 0.28 m^2/gC), indicating that hydrophobic OC possesses a stronger light-absorbing capacity than hydrophilic OC. Biomass burning (31.0%) and coal combustion (31.1%) were the dominant sources of WIOC, with coal combustion sources exhibited the strongest light-absorbing capacity. Moreover, employing the simple forcing efficiency ($SFE_{300\text{-}700nm}$) method, we observed that WIOC exhibited the highest $SFE_{300\text{-}700nm}$ (6.57 ± 5.37 W/g) among the EX-OC fractions. The radiative forcing of EX-OC was predominantly contributed by hydrophobic OC (WIOC: $39.4 \pm 15.5\%$ and HULIS: $39.5 \pm 12.1\%$). Considering the aromaticity, sources, and atmospheric processes of different carbonaceous components, we propose a light-absorbing carbonaceous continuum, revealing that components enriched with fossil sources tend to possess stronger light-absorbing capacity, higher aromatic levels, increased molecular weights, and greater recalcitrance in the atmosphere. Reducing fossil fuel emissions emerges as an effective means of mitigating both gaseous (CO_2) and particulate light-absorbing carbonaceous warming components.

Highlights

- WIOC contributed significantly to both concentrations and the light absorption efficiency of extractable organic carbon.
- WIOC is primarily originated from biomass burning and coal combustion in China.
- WIOC displayed the highest radiative forcing among the extractable organic fractions.
- Carbonaceous components that are more enriched with fossil sources tend to exhibit stronger light-absorbing capacity, higher aromatic levels and molecular weight, and enhanced recalcitrance

1. Introduction

Organic carbon (OC) constitutes a substantial fraction (20 to 90%) of carbonaceous aerosols, playing an important role in human health, air quality and climate change (Jimenez et al., 2009; Zhang et al., 2007). Recent studies have shown that specific organic compounds could efficiently absorb radiation in near-ultraviolet (UV) and visible spectral regions, exhibiting a strong wavelength dependence (Laskin et al., 2015; Andreae and Gelencser, 2006). Due to its brownish or yellowish visible appearance, the light-

absorbing OC is term as brown carbon (BrC) (Sun et al., 2007; Saleh, 2020). Currently, model studies showed that the BrC account for ~20 to 40% of the light absorption of total carbonaceous aerosols absorption globally, hence, BrC has the potential to counteract the cooling effects of OC, introducing considerable uncertainty into climate models (Bahadur et al., 2012; Feng et al., 2013; Saleh et al., 2015). Moreover, BrC may contribute to the generation of reactive oxygen species (ROS) in ambient aerosols, posing potential adverse effects on human health (Verma et al., 2012; Wang et al., 2023). To comprehensively understand and address the climate and health impacts of BrC, there is a critical need for thorough investigations into the sources and light-absorbing properties of OC.

According to water solubility, OC can be classified into two main categories: water-soluble OC (WSOC) and water-insoluble OC (WIOC). While WSOC has been extensively studied over the past decades, with investigations focusing on its sources, light-absorbing properties, and atmospheric processes (Bosch et al., 2014; Dasari et al., 2019; Mo et al., 2021; Wozniak et al., 2014; Wang et al., 2020). WIOC, which makes up large fraction of OC (~up to 80%) and a substantial portion of light absorption by BrC, has received comparatively less attention. WIOC exhibits a significantly higher light-absorbing capacity compared to WSOC, attributed to the enrichment of strong light-absorbing BrC chromophores in WIOC. For instance, certain strong BrC chromophores like polycyclic aromatic hydrocarbons (PAHs) and their derivatives, as well as high-molecular-weight oligomers, are water-insoluble (Huang et al., 2020; Xie et al., 2017; Kalberer et al., 2006). Indeed, Zhang et al. (2013) reported that the light absorption by methanol-extracted OC in Los Angeles was approximately 3 and 21 times higher than that by WSOC. Moreover, field observations indicate that WIOC exhibits greater recalcitrance during long-range transport processes compared to WSOC, leading to a longer lifetime for WIOC (Wozniak et al., 2012; Fellman et al., 2015; Kirillova et al., 2014). Given that WIOC represents a relatively long-lived OC component with a higher light-absorbing capacity, a comprehensive understanding of its sources and light-absorbing properties is imperative.

China as the hotpot regions of OC, the columnar mass concentration of BrC in China (4.4 to 92 mg/m^2) is much higher than those in Europe and U.S.A (~5 mg/m^2) (Arola et al., 2011; Zhang et al., 2017). While the sources and light-absorbing properties of WSOC have been extensively investigated in China (Huang et al., 2020; Jiang et al., 2020b; Wang et al., 2023; Cheng et al., 2016; Yan et al., 2017; Mo et al., 2021), corresponding information on WIOC remains limited, especially on a national scale. In this study, we

selected ten representative Chinese cities with urbanization rates ranging from 37.8% to 88.0% to represent the regions with different developed levels. The primary objectives are to explore the spatiotemporal variations in concentrations, light absorption properties, sources, and radiative effects of WIOC across these urban areas. Additionally, we integrate and make a comparison of light-absorbing properties data (mass absorption efficiency [MAE] and absorption Ångström exponent [AAE]) of OC with different polarities and BC from previous studies (Mo et al., 2021; Mo et al., 2024). This includes hydrophobic WSOC isolated by solid-phase extraction (SPE) referred to as humic-like substances (HULIS) and the hydrophilic WSOC referred to as non-HULIS. Finally, we propose a continuum concept of light-absorbing carbonaceous aerosols linked to aromaticity, sources, and atmospheric processes. This study provides insights into light-absorbing properties and sources of WIOC, contributing essential knowledge for a comprehensive understanding the role of WIOC in climate forcing and developing strategies to mitigate its climate impact.

2. Materials and Methods

2.1 Sampling

PM$_{2.5}$ samples were collected across four seasons in ten cities in China. These cities included four with central heating systems (Beijing, Xinxiang, Lanzhou, and Taiyuan) and six without central heating (Shanghai, Nanjing, Chengdu, Guiyang, Wuhan, and Guangzhou), as shown in Figure 1. All the filter samples were collected on pre-combusted (450℃, 6h) quartz-fiber filter (Pall, England) from 2013 to 2014, use a high-volume sampler at a flow rate of ~ 1000L/min. Detailed information about the sampling methods can be found in our previous study (Mo et al., 2021; Mo et al., 2024). In brief, each sampling campaign spanned approximately 30 days for fall, winter, spring, and summer, respectively. Subsequently, a 20 mm diameter sample was excised from each filter during every season, and these were amalgamated into a single sample, with the exception of Guiyang, where only fall and winter samples were available. A total of 38 pooled samples were utilized in subsequent experiments. For each location, one pooled sample was obtained for each season, thus providing analytical results representing seasonal averages.

114 .
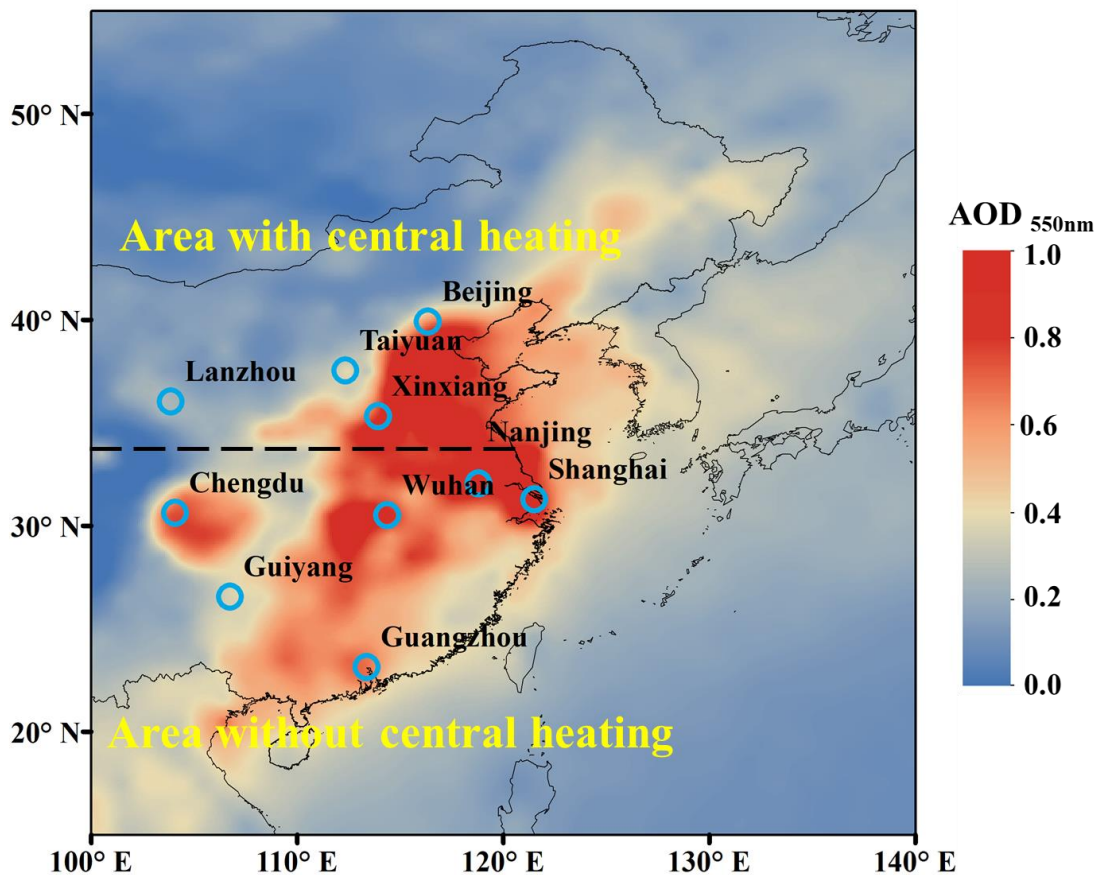
Figure 1. The average aerosol optical depth (AOD) at 550 nm retrieved from satellite (Terra/MODIS) observations over East Asia during October 2013 to August 2014. The locations of ten Chinese cities are shown in the map. Beijing, Xinxiang, Lanzhou and Taiyuan located in the areas with central heating in cold seasons (fall and winter). Shanghai, Nanjing, Chengdu, Guiyang, Wuhan and Guangzhou located in the areas without central heating. The average annual temperature of with central heating the area with is usually below 15 °C, while the areas without central heating is usually higher than 15 °C.

2.2 Chemical analysis

For water-soluble inorganic ions analysis, the filters were ultrasonically extracted with ultrapure water (18.2 MΩ cm) in a polypropylene vial for 30 min. Extracts were filtered through polytetrafluoroethylene (PTFE) syringe filters (Jinteng Ltd., Tianjin, China) of 0.22 μm pore size to remove particles and filter debris. Seven water soluble inorganic ions (Na^+, NH_4^+, K^+, Ca^{2+}, Cl^-, SO_4^{2-}, and NO_3^-) were determined by ion-chromatography (761 Compact IC, Metrohm, Switzerland, Text S1). The detection limit was below 0.05 mg/L for all ions.

For the solvent extraction, the water-soluble organic carbon (WSOC) in the pooled sample was

extracted with 100 mL ultrapure water (18.2 MΩ, Sartorius) under ultrasonication (30 min × 3 times). Following previous studies demonstrating that most water-insoluble organic carbon (WIOC) can be extracted in methanol (> 90%) (Chen and Bond, 2010; Chen et al., 2017; Cheng et al., 2016), the same sample underwent drip drying, and the WIOC was re-extracted methanol (OCEANPAK, HPLC-Grade, 30 min × 3 times) using the same procedure. Both the methanol and water extracts were filtered through a 0.22 μm PTFE membrane to remove insoluble particles. Both the methanol and water extracts were filtered through a 0.22 μm PTFE membrane to remove insoluble particles. The WSOC further separated into a relatively hydrophobic (humic-like substance, HULIS) and hydrophilic (non-HULIS) fraction (Lin et al., 2010a; Fan et al., 2012). HULIS are operationally defined by the procedure used for isolation from bulk WSOC by removing low molecular weight organic acids and inorganic ions. The HLB (Oasis, 30 μm, 60 mg/cartridge, Waters, USA)-SPE method is most widely used to isolate HULIS due to its excellent reproducibility and high recovery yield (Fan et al., 2012; Lin et al., 2010b). Therefore, we used an HLB-SPE column to isolate the HULIS.

The WSOC and HULIS-C content was determined using a TOC analyzer equipped with a nondispersive infrared (NDIR) detector (Shimadzu TOC-VCPH, Japan). The non-HULIS-C was estimated by the difference between WSOC and HULIS-C (non-HULIS-C = WSOC - HULIS-C). For WIOC measurement, 40 mL methanol extracts were evaporated to dryness under a nitrogen stream and re-dissolved with 1.0 mL methanol. A 20 μL aliquot of extracts was slowly spiked onto a 1.5 cm^2 prebaked quartz filter. After methanol evaporation, carbon on the quartz filter was quantified with an OC/EC analyzer (Sunset Laboratory Inc). The carbon contents of WIOC were determined by an OC/EC analyzer with standard deviation of reproducibility test less than 3%. The analysis mechanism of OC/EC analyzers and TOC analyzers differ, including the different catalysts and detectors they employ. However, it is important to note that both OC involve converting carbon in the sample to CO_2 and detecting CO_2 using a nondispersive infrared detector (NDIR) or a flame ionization detector (FID) after CO_2 conversion to methane. Thus, the analytical mechanisms are similar. Indeed, previous studies have systematically compared these two methods for determining WSOC in aerosols (Yu et al., 2002). The results have demonstrated no significant differences between the measurements obtained from the two methods. Therefore, the carbon content of various carbonaceous components determined by these two methods should be comparable. Based on extractable OC (EX-OC) polarity, the EX-OC was separated into WIOC, HULIS-C, and non-HULIS-C. All WSOC, HULIS-C, and WIOC concentrations presented in this study

162 were corrected with field blanks (0.39 ± 0.16, 0.66 ± 0.21, and 1.75 ± 0.48 µgC/cm^2, respectively).

163

2.3 Light absorption spectra measurement

165 The absorption spectra of sloven extracted fractions were recorded from 200 to 800 nm relative to

166 ultrapure water by a UV-visible spectrophotometer (UV-4802, Unico, China). The light absorption

167 coefficient was calculated according to following equation (Hecobian et al., 2010; Kirillova et al., 2014):

168 $$Abs_\lambda = (A_\lambda - A_{700}) \frac{V_l}{V_a \times l} \times \ln(10) \qquad (1)$$

169 where Abs_λ is the light absorption coefficient (Mm^{-1}), V_l is the volume of solvent for extraction

170 (ml), V_a is the volume of sampled air (m^3), l is the optical path length (in this case, 0.01 m), and A_λ is the

171 absorption of the solution at a given wavelength. The average light absorption between 695 and 705 nm

172 (A_{700}) was used to account for baseline drift during analysis. The mass absorption coefficient (MAE, m^2/gC)

173 of sloven extracted OC fractions at wavelength of λ can be calculated as:

174 $$MAE_\lambda = \frac{Abs_\lambda}{C_i} \qquad (2)$$

175 Where C_i is the corresponding concentration of WIOC, HULIS-C and non-HULIS-C in the air

176 (µgC/m^3).

177 The wavelength dependence of different OC fraction can be investigated by fitting the absorption

178 Ångström exponent (AAE) by the following relation:

179 $$Abs_\lambda = K \times \lambda^{-AAE} \qquad (3)$$

180 The AAE is calculated by a linear regression of ln (Abs_λ) on ln(λ) within the range 330-400 nm for

181 the avoidance of interference by non-organic species (e.g., NO$_3^-$). The ratio of light absorption at 250 and

182 365 nm (E2/E3), which is negatively correlated with aromaticity and molecular weight of organics was

183 also calculated (Peuravuori and Pihlaja, 1997; Baduel et al., 2010).

184

2.4 Positive matrix factorization (PMF) source apportionment

186 We applied U.S EPA PMF 5.0 model to qualitatively and quantitatively identify sources of WIOC and

187 $Abs_{365, WIOC}$ in this study. The principle and detailed process of this model could be found in Paterson (1999)

188 and EPA 5.0 Fundamentals & User Guide. PMF model is a commonly used mathematical approach for the

189 apportionment of PM$_{2.5}$ sources abase on the characteristic chemical compositions or fingerprints in each

190 source. The model decomposes the concentrations of the chemical species of samples (X) into sets of

contributions (G), factor profiles (F), and residuals (E):

$$X = G \times F + E \quad (4)$$

During the model calculation, factor contributions and profiles were derived by minimizing the objective function Q in PMF model:

$$Q = \sum_{i=1}^{m} \sum_{j=1}^{n} \left(\frac{E_{ij}}{\sigma_{ij}} \right)^2 \quad (5)$$

where E_{ij} is the residual of each sample, and σ_{ij} is the uncertainty in the jth species for the sample i.

The measurement uncertainties were used for the error estimates of the measured concentrations. Data values below the method detection limit (MDL) were substituted with MDL/2. Missing data values were substituted with median concentrations. If the concentration is less than or equal to the MDL, the corresponding uncertainty (Unc) is 5/6 MDL. Otherwise, the uncertainty is calculated following equation:

$$Unc = \sqrt{(error\ fraction \times concentration)^2 + (0.5 \times MDL)^2} \quad (6)$$

We performed 100 random runs and retained the runs that produced minimum Q values for 3 to 10 factors in base runs, five factors were obtained as the optimal solution as the source profiles in this study (Figure S1). The errors associated with both random and rotational ambiguity in the PMF solution were assessed using the bootstrap (BS) model and the displacement (DISP) model. The BS model involves estimating errors by resampling data matrices, with the resulting BS factors being aligned with the base run factors to gauge the reproducibility of different factors amidst random errors. Analysis using a 4-factor BS model indicated a factor mapping exceeding 85%, suggesting both the suitability of the number of factors and the presence of uncertainties. On the other hand, DISP primarily investigates rotational ambiguity within the PMF outcomes. Notably, in the context of a 4-factor PMF model, no swaps were identified in the DISP analysis.

2.5 Radiative effect calculation

The "simple forcing efficiency" (SFE, W/g) proposed by Bond and Bergstrom (2006) was used to estimate the potential direct radiative effects caused by light-absorbing OC. The SFE was originally used to represent the normalization of the particle mass (Chylek and Wong, 1995). Here, we focused on the light absorption effect of OC without the scattering effect. A wavelength-dependent SFE of light-absorbing OC as follows (Chen and Bond, 2010) :

$$\frac{dSFE_{abs}}{d\lambda} = D \frac{dS(\lambda)}{d\lambda} \tau_{atm}^2 (1 - F_c) \times 2\alpha_s \times MAC_i \tag{7}$$

where S and τ_{atm} refer to solar irradiance and atmospheric transmission, respectively, with both being from ASTM G173–03 reference spectra (W/m^2). D is the daytime fraction (0.5), Fc is the cloud fraction (0.6), and α_s is the surface albedo (0.19 for Earth average). MAC_i is mass absorption cross section of sloven extracted OC (e.g., WIOC, HULIS and non-HULIS). Note that MAC refers to the particulate absorption per mass, while MAE is derived from absorption of the aqueous extracts. MAC can be compared with MAE only after considering the particulate effect (Sun et al., 2007) (Text S2). And then, the fraction of solar radiation absorbed by OC component with different polarity relative to total EX-OC is calculated as:

$$f_{OC_i/EX\_OC} = \frac{\sum_{\lambda=300}^{700} SFE_{OC_i}(\lambda) \times C_i \times \left(\frac{OA}{OC}\right)}{\sum \sum_{\lambda=300}^{700} SFE_{OC_i}(\lambda) \times C_i \times \left(\frac{OA}{OC}\right)} \tag{8}$$

Here, the integrated SFE is the sum of the SFE from 300 to 700 nm; C_i is the corresponding concentration of WIOC, HULIS-C and non-HULIS-C in the air (μgC/m^3). The OA/OC ratios are 1.51, 1.91, 2.30 for WIOC, HULIS and non-HULIS, respectively (Kiss et al., 2002).

3. Results and Discussion

3.1 Spatiotemporal variations in WIOC concentration and light-absorbing properties

In this study, water-insoluble organic carbon (WIOC) is defined as the residual OC re-extracted by methanol after water extraction, representing the OC only soluble in methanol. We define the OC extracted by water from the aerosol filter sample as WSOC, the WSOC is further separated into hydrophobic fraction (HULIS-C) and hydrophilic fraction (non-HULIS-C). The combined sum of WSOC and WIOC is defined as extractable OC (EX-OC). Figures 2 shows the spatial variation of concentration and Abs$_{365}$ of separated EX-OC fractions across ten Chinese. The concentrations of WIOC ranged from 1.45 to 12.95 μgC/m^3, with an average of 3.64 ± 2.53 μgC/m^3 (average ± one standard deviation) among the 10 cities (Figure 2a). Specifically, the areas with central heating exhibited significantly higher average WIOC concentrations compared to areas without central heating (4.79 ± 3.39 μgC/m^3 vs. 2.81 ± 1.16 μgC/m^3, $p < 0.01$), likely attributed to coal and biofuel combustion for domestic/central heating during the cooler period (Wang et al., 2023; Wang et al., 2020). Despite substantial spatial variation in WIOC concentration, its contribution

to EX-OC remained consistent at 33.4 ± 7.6%, showing no significant spatial or temporal variations. Furthermore, the fractional carbon mass contributions of WIOC (33.4 ± 7.6%), HULIS-C (35.2 ± 5.8%), and non-HULIS-C (31.4 ± 5.2%) to EX-OC were similar (Figure 2 and Table S1).

Consistent with spatial variation in WIOC concentration, the Abs_{365} of WIOC ($Abs_{365, WIOC}$) serving as a proxy for BrC were significantly higher in areas with central heating compared to those without central heating (10.1 ± 10.3 Mm^{-1} vs. 4.41 ± 2.68 Mm^{-1}, p < 0.01). Notably, the light absorbing contribution of WIOC (40.5 ± 9.73%) to EX-OC exceeded its corresponding carbon mass contribution (33.4 ± 7.55%). Actually, the light absorbing contribution of EX-OC are largely contributed by relatively hydrophobic OC components: the WIOC (40.5 ± 9.73%) and HULIS (41.6 ± 7.28%). In contrast, the non-HULIS fraction, being the most polar, contributed only 17.5 ± 5.02% to $Abs_{365, EX-OC}$ (Table S1). This suggests that the majority of light-absorbing organic compounds were enriched in the WIOC and HULIS fractions. Therefore, the mean mass absorption efficiency (MAE) spectra of WIOC and HULIS, representing the light-absorbing capacity per unit carbon mass, were higher than those of non-HULIS (Figure 2c).
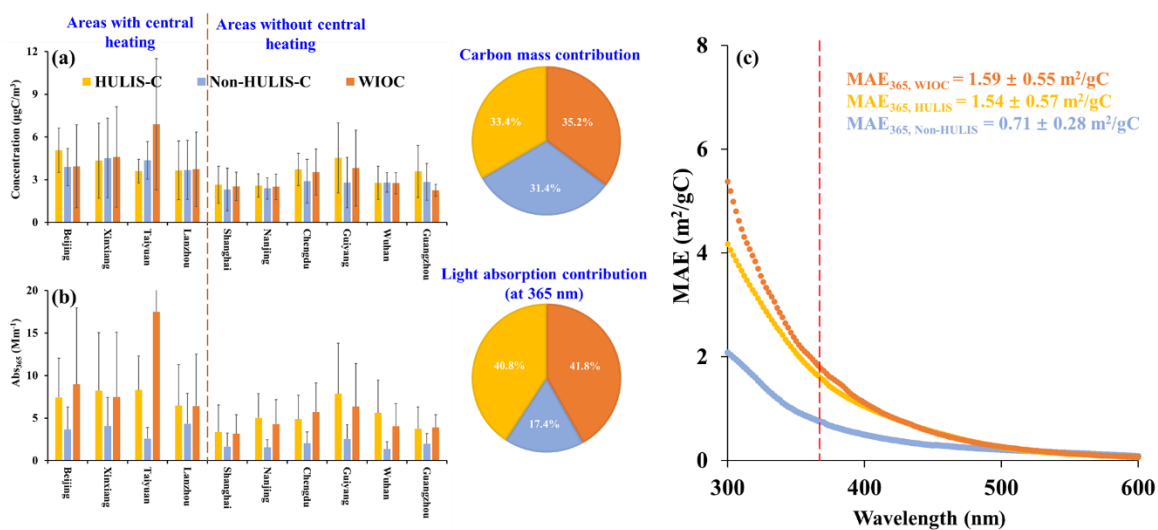
Figure 2. The spatial variation of concentration and light absorption of extractable OC from ten Chinese cities. (a) The spatial variations of concentration of WIOC, HULIS-C and non-HULIS-C in $PM_{2.5}$ from ten Chinese cities; (b) The spatial variations of light absorption coefficients of WIOC, HULIS-C and non-HULIS-C at 365 nm (Abs_{365}) in $PM_{2.5}$ from ten Chinese cities; The pie charts in the left of panel (a) and (b) represent the carbon mass contribution and light absorption contribution, respectively. (c) The mean of mass absorption efficient (MAE) of WIOC, HULIS and non-HULIS from 300 nm to 600 nm; The red dash line represents the MAE_{365}.

271

The MAE at 365 nm (MAE_{365}) is commonly used to reflect the light-absorbing capacity of solvent extracted-BrC. Among the extractable OC components, the MAE_{365} of WIOC is the highest, with average of 1.59 ± 0.55 m^2/gC. This value is comparable to the WIOC in Xi'an (1.5 ± 0.5 m^2/gC) and Beijing (1.5 ± 0.4 m^2/gC) (Huang et al., 2020), but ~5 times higher than values reported in Nagoya, Japan (0.2 to 0.4 m^2/gC) (Chen et al., 2016). The MAE_{365} of WIOC is comparable to HULIS (1.54 ± 0.57 m^2/gC), however, higher than the non-HULIS as relatively polar water-soluble fraction (0.71 ± 0.28 m^2/gC). This discrepancy is likely attributed to the non-HULIS fraction mainly comprising highly oxidized organic matter lacking long aromatic conjugated systems (Chen et al., 2017; Chen et al., 2016). It should be noted that light absorption of BrC, as measured by solvent extraction, appears to be underestimated compared to under ambient aerosol conditions. To accurately derive the corresponding BrC absorption in ambient aerosols, it is necessary to calibrate the absorption determined in solvent extracts using a correction factor. Presently, the correction factor proposed by Liu et al. (2013), typically set at 2, is widely employed for this purpose. Despite WIOC being recognized as the most light-absorbing OC component, even after applying this correction factor, we observed that the MAE of WIOC at 550 nm(0.28 ± 0.09 m^2/gC) remains an order of magnitude lower than that of amorphous tar ball BrC (approximately 3.6 to 4.1 m^2/g) and unextractable "dark BrC" (approximately 1.2 m^2/g) as determined by transmission electron microscopy (Alexander et al., 2008; Chakrabarty et al., 2023), indicating the light-absorbing capacity of the extractable OC is relatively weakly.

The MAE_{365} of WIOC exhibited significant seasonal variation, with higher values in cold seasons (1.74 ± 0.64 m^2/gC, fall and winter) than in warm seasons (1.48 ± 0.46 m^2/gC, spring and summer, Figure 3a). This variation is likely linked to changes in sources and atmospheric processes influencing the light-absorbing compounds within the WIOC fraction. During cold seasons, large usage of coal combustion and biomass burning (BB) for central/domestic heating may elevate the emission of the WIOC with high MAE_{365} (Tang et al., 2020; Song et al., 2019), consequently enhancing the overall MAE_{365} of WIOC. Conversely, stronger photobleaching effects and lower emissions from coal combustion and BB during warm seasons may contribute to a decrease of MAE_{365} of WIOC (Saleh et al., 2013; Wong et al., 2017). Interestingly, all extractable OC components exhibit a consistent seasonal pattern (cold > warm) in their MAE_{365}, indicating similar influences of sources and atmospheric processes on the light-absorbing capacity of these components irrespective of polarity. Spatially, the MAE_{365} of WIOC was significantly higher in

areas with central heating than without central heating (1.75 ± 0.64 m²/gC vs. 1.48 ± 0.46 m²/gC, $p < 0.01$). The difference in MAE_{365} of WIOC between the areas with and without central heating was more pronounced during colder seasons (2.20 ± 0.51 m²/gC vs. 1.81 ± 0.28 m²/gC, 21.5% difference) than warmer seasons (1.29 ± 0.37 m²/gC vs. 1.17 ± 0.26 m²/gC, 10.3% difference). Given that coal consumption for central/domestic heating is considerably higher in areas with central heating compared to those without, it is plausible that the spatial variability in MAE_{365} of WIOC is predominantly influenced by coal combustion.

The distinct seasonal variation of light-absorbing capacity of WIOC may be affected by the structure of light-absorbing compounds within WIOC. AAE reflects both the wavelength dependent light absorption and aromaticity of the carbonaceous aerosols, and the AAE usually negatively related with the aromaticity (Chen et al., 2017; Mo et al., 2017; Zhang et al., 2013). BC as most condensed aromatic and strongest light-absorbing carbonaceous, exhibits an AAE of ~1 (Bond, 2001; Kirchstetter et al., 2004). In the case of BrC in solvent extracts, AAE values typically vary from ~3 to 16 (Hecobian et al., 2010; Mo et al., 2021; Chen and Bond, 2010). Generally, During photobleaching aging processes, the MAE of BrC in solvent extracts tends to decrease with increasing AAE values, indicative of a reduction in aromaticity (Dasari et al., 2019). Despite the stronger radiation and lower MAE_{365} of WIOC in warm seasons, AAE values did not exhibit seasonal variation (4.59 ± 0.52 vs. 4.77 ± 0.65, $p > 0.05$, Figure 3b). This may be due to the more complex factors affecting the AAE values, which are not only affected by sources and atmospheric processes (Saleh et al., 2013; Tang et al., 2020; Dasari et al., 2019), but also by the solvents and the pH of water extracts applied in the determination (Chen et al., 2016; Mo et al., 2017; Phillips et al., 2017). However, the AAE values for WIOC (4.69 ± 0.59) were comparable to those of HULIS (4.72 ± 0.53) but lower than those of non-HULIS (7.33 ± 2.56). This suggests a tendency for AAE to increase with the polarity of OC components, in agreement with findings from Los Angeles and Nagoya (Chen et al., 2016; Zhang et al., 2013). This indicated that relatively hydrophobic fractions (e.g., WIOC and HULIS) contain more aromatic light-absorbing compounds than non-HULIS.

In contrast, the seasonal variation is more pronounced for the ratio of light absorption at 250 and 365 nm (E2/E3), inversely proportional to the molecular weight (MW) and aromaticity of natural organic matter (Baduel et al., 2010; Peuravuori and Pihlaja, 1997). The E2/E3 of WIOC was lower in cold seasons compared to warm seasons (4.33 ± 0.49 vs. $4.51 \pm 0.0.48$, $p < 0.01$, Figure 3c), suggesting the WIOC

exhibited greater conjugations and aromaticity in cold seasons. Notably, the E2/E3 ratio exhibits a stronger correlation with combustion source tracers (e.g., K^+ and Cl^-) during cold seasons (K^+: r = 0.37, p = 0.02 vs. r = 0.34, p > 0.1; Cl^-: r = 0.56, p = 0.011 vs. r = 0.16, p > 0.1) than in warm seasons, indicating that coal combustion and BB contribute to higher aromaticity of WIOC during cold seasons (Duarte et al., 2005; Fan et al., 2016). Indeed, coal combustion and BB are important sources of OC with high level aromatic compounds (e.g., PAHs). Additionally, the slower photo-degradation and volatilizations of aromatic compounds in lower temperature also enhanced the aromatic level of WIOC in cold seasons (Samburova et al., 2007; Zhang et al., 2020b). Similar to AAE, the E2/E3 of extractable OC components exhibited a consistent trend of increasing with the polarity of OC (WIOC: 4.41 ± 0.49 < HULIS: 4.93 ± 0.50 < non-HULIS: 7.00 ± 0.42, p < 0.01), suggesting that less polar organics likely have higher aromaticity and higher MW. However, in contrast to AAE, all E2/E3 ratios of the EX-OC components exhibited the same seasonal variation (cold > warm, Figure 3c). This implies that the E2/E3 ratio, calculated using two wavelengths, maybe more effective than the AAE calculated using multiple wavelengths when reflecting changes in the structure of organic components. The seasonal variation in the structure and light-absorbing properties of WIOC is largely influenced by sources, we further explore the source of WIOC, as discussed below.
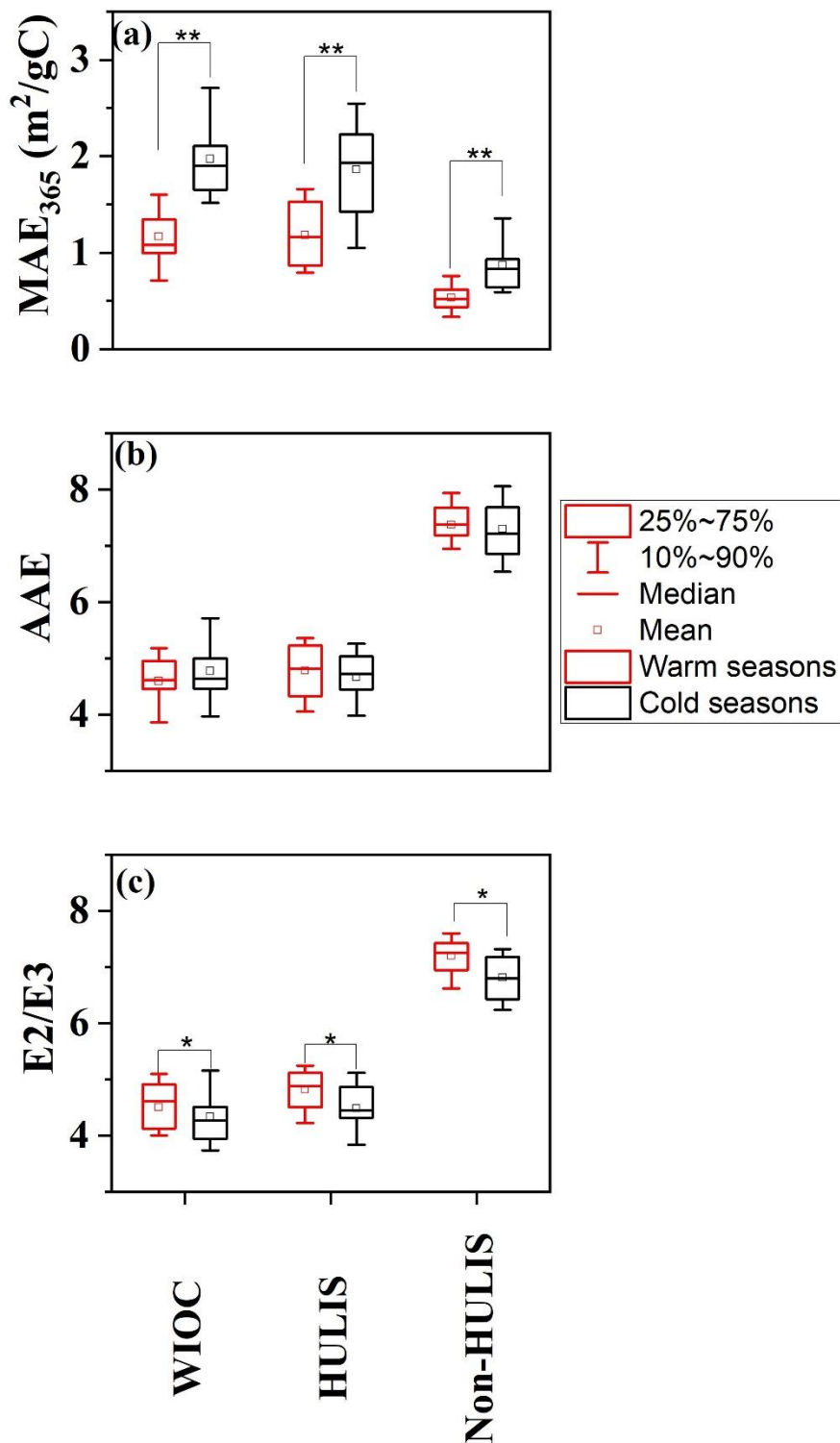
349

Figure 3. The seasonal variations of (a) AAE, (b) E2/E3 and (c) MAE_{365} for the WIOC, HULIS and

WSOC. "*" indicates the difference at $p < 0.05$ level; "**" indicates the difference at $p < 0.01$ level

352

3.2 The sources of WIOC: coal combustion exhibited the strongest light-absorbing capacity

In order to better understand the source of WIOC and BrC in WIOC fraction, correlation of WIOC and

Abs$_{365, \text{WIOC}}$ to water-soluble ions were investigated. Although the WIOC exhibited strong correlation with Abas$_{365, \text{WIOC}}$ (r = 0.97, $p < 0.01$) for the entire year, as listed in Table S2, the correlations between WIOC and Abs$_{365, \text{WIOC}}$, as well as WIOC and water-soluble ions, differed notably between warm and cold seasons. This discrepancy suggests differences in sources and formation processes of WIOC and light-absorbing compounds between warm and cold season. During cold seasons, both WIOC and Abs$_{365, \text{WIOC}}$ exhibited good relationship with most of the water-soluble ions (Table S2). Conversely, in warm seasons, WIOC showed poor correlation with most water-soluble ions, except for NH$_4^+$ (r = 0.51, $p < 0.05$). Compared with the WIOC, the Abs$_{365, \text{WIOC}}$ correlated well with most water-soluble ions (r = 0.63, 0.53, 0.51 and 0.59 for Cl$^-$, NO$_3^-$, SO$_4^{2-}$, and NH$_4^+$, respectively, $p < 0.05$, Table S2), except the K$^+$ (r = 0.25, $p > 0.05$), in warm seasons. This suggests that the difference in sources and formation processes in WIOC and light-absorbing compounds in warm seasons.

To better quantify the seasonal variation of the sources of WIOC and BrC in WIOC fraction, we quantified the sources for both WIOC concentrations and light absorption of WIOC (Abs$_{365, \text{WIOC}}$) using the PMF receptor model in this study. The model identified five factors with uncertainties below 12%, and their profiles are presented in Figure S1. Factor 1 exhibited a high Cl$^-$ loading (57.0%), which a typical tracer for BB, coal combustion and sea-salt aerosols. Sea-salt derived Cl$^-$ is considered as a significant source of Cl$^-$ in PM$_{2.5}$ in coastal cities. In this study, we assessed the contribution of sea-salt Cl$^-$ ([ss-Cl$^-$] =[ss-Cl$^-$] = 1.17 × [Na$^+$]) to the total Cl$^-$. We found that even in the coastal cities, such as Guangzhou and Shanghai, the contribution of sea-salt Cl$^-$ to total Cl$^-$ was generally below ~7%. Thus, the high loading of Cl$^-$ is not likely caused by the sea-salt aerosols. K$^+$ as typical tracer for BB, the loading of K$^+$ (11.7%) was relatively low in Factor 1. Further, Factor 1 displayed a ratio of Abs$_{365, \text{WIOC}}$ to WIOC (2.46 m^2/gC) comparable to the MAE$_{365}$ of WIOC from coal combustion (Tang et al., 2020). Consequently, Factor 1 was classified as a source related to coal combustion. Factor 2 was characterized by the highest loading of K$^+$ (45.8%) and HULIS-C (44.1%), thus, this factor was identified as BB. Factor 3 exhibited enrichment in SO$_4^{2-}$ (46.0%) and non-HULIS-C (18.2%), both recognized as key components in atmospheric aging processes (Du et al., 2014). Notably, the ratio of Abs$_{365, \text{WIOC}}$ to WIOC in Factor 3 was the lowest (0.55 m^2/gC) among the identified factors. This observation suggests a probable loss of light-absorbing capacity during aging/bleaching processes. Thus, Factor 3 is interpreted as the source associated with aging processes. Factor 4 is related to high loading of NO$_3^-$ (56.2%) and NH$_4^+$ (34.8%). Given that SOA formed under high NO$_x$/NH$_3$ conditions often exhibits high light-absorbing capacity (Xie et al., 2017; Lin et al.,

2018), and considering the relatively high ratio of $Abs_{365, WIOC}$ to WIOC (2.13 m^2/gC) observed in Factor 4, we attribute Factor 4 to be a source related to nitrogen-induced SOA formation. Factor 5, characterized by the highest loading of Ca^{2+} (65.7%). Ca is identified as tracer of fugitive dust (Han et al., 2007). The predominance of Ca in Factor5, which points to sources such as resuspended dust and soil sources. Both the predicted WIOC concentrations ($R^2 = 0.92$) and $Abs_{365, WIOC}$ ($R^2 = 0.91$, Figure S2) correlated well with the corresponding measured values, confirming the reliability of PMF solution.

Figure 4a shows the annual average contributions of the identified sources to WIOC resolved by PMF model. The primary sources of WIOC were combustion sources, with coal combustion and BB averagely account for 31.1% and 31.0% of the WIOC, respectively. Although the contribution of coal combustion to WIOC was comparable to that of BB, both exhibited distinct spatial and seasonal variations (Figure 4a). Specifically, during winter, coal combustion emerged as the dominant source of WIOC, accounting for 48.4% of the total, likely driven by increased coal usage in areas with central heating. Indeed, coal combustion constituted the primary source of WIOC in areas with central heating during cold seasons (56.2%). In contrast, in areas without central heating, the contribution of BB surpassed that of coal combustion significantly (54.2% vs. 17.3%). Therefore, coal combustion and BB were identified as the predominant sources of WIOC in areas with and without central heating, respectively, during cold seasons. Compared to primary emissions sources, the contributions of the sources related to aging processes and nitrogen-induced secondary formation were relatively lower, accounting for 18.2% and 5.2% of the WIOC, respectively. That may be due to these two secondary sources are more enriched in water-soluble components (HULIS-C + non-HULIS-C). Actually, although the uncertainties of sources contribution of HULIS-C and non-HULIS-C resolved by PMF model may be high, the aging processes and nitrogen-related secondary formation contributed 10.1% and 20.2% to HULIS-C, and 18.3% and 21.6% to non-HULIS-C, respectively. In addition, during the summer, when both temperature and solar radiation intensity rise, the contributions from aging processes and BB increased to 39.3% and 41.3%, respectively. In spring, a significant fraction of WIOC was associated with dust/soil, reaching up to 28.8%. Specially, the dust/soil contribution was much higher in the areas with central hearing than those without central heating. This is consistent with the fact that sandstorms from the Gobi desert that borders China and Mongolia ride springtime winds to affect the air quality of Northern China (Filonchyk et al., 2024).

Figure 4c shows the contributions of sources identified by PMF model to the $Abs_{365, WIOC}$. Generally,

coal combustion (46.5%) and BB (30.0%) dominate $Abs_{365, WIOC}$, while other sources just contribute 23.8% (aging processes: 6.1%, nitrogen-related secondary formation: 6.7%, and dust/soil: 10.8%) of $Abs_{365, WIOC}$. Annually, even though the mass contributions of coal combustion and BB to WIOC are comparable, coal combustion is the largest contributor to $Abs_{365, WIOC}$, surpassing BB. This difference is likely because coal-derived WIOC has a stronger light-absorbing capacity than BB. The seasonal variation of sources contribution of $Abs_{365, WIOC}$ is similar to that of carbon mass contribution. Coal combustion is the dominant contributor to $Abs_{365, WIOC}$ in winter (62.5%), but its contribution diminishes in other seasons, suggesting that the enhanced light absorption of WIOC in winter is driven by coal combustion. In summer, the elevated solar radiation and temperatures can promote the secondary generation of BrC, with secondary BrC being more enriched in the WSOC. Previous studies have observed a significant contribution of secondary sources to WSBrC during summer (Yan et al., 2017; Du et al., 2014). However, the BrC within WIOC tends to be more enriched with primary sources such as BB and coal combustion (Figure 4c). As temperatures rise in summer, coal consumption typically declines. Consequently, during summer, $Abs_{365, WIOC}$ is predominantly contributed by BB (Figure 4d). In spring, the contribution of dust/soil to $Abs_{365, WIOC}$ reaches up to 26.6%, likely due to the presence of humic substances with strong light-absorbing capacity in dust/soil (Andreae and Gelencser, 2006).

The source of BrC significantly influences its light absorption capacity. For WIOC, the contribution from aging processes shows a negative correlation with the MAE_{365} of WIOC (r = -0.61, $p < 0.01$, Figure S3a), indicating that the chromophores in WIOC were bleached during aging processes. Both BB and coal combustion are recognized as the sources of BrC with strong light-absorbing capacity. We found that contribution of BB exhibited a negative correlation with $MAE_{365, WIOC}$ (r = -0.34, p = 0.46, Figure S3b), whereas a strong positive correlation was observed for coal combustion (r = 0.72, $p < 0.01$, Figure S3a). These suggest that the light-absorbing compounds derived from coal combustion have a stronger light-absorbing capacity than BB, and enhanced the overall $MAE_{365, WIOC}$. Moreover, the contribution from coal combustion is also significantly positively correlated with the light absorption contribution of WIOC to EX-OC ($Abs_{365, WIOC}/Abs_{365, EX-OC}$, r = 0.46, $p < 0.01$, Figure S3c). This implies that the strong light-absorbing compounds emitted from coal combustion tend to be water-insoluble. It is noteworthy that, based on carbon isotopes ($\delta^{13}C$ and $\Delta^{14}C$), coal combustion is identified as the major source of strong light-absorbing components in the water-soluble fraction in China (Mo et al., 2021; Mo et al., 2024). Therefore, coal combustion is the dominant source of EX-OC with strong light-absorbing capacity in China, which

449 enhances the overall color of EX-OC.
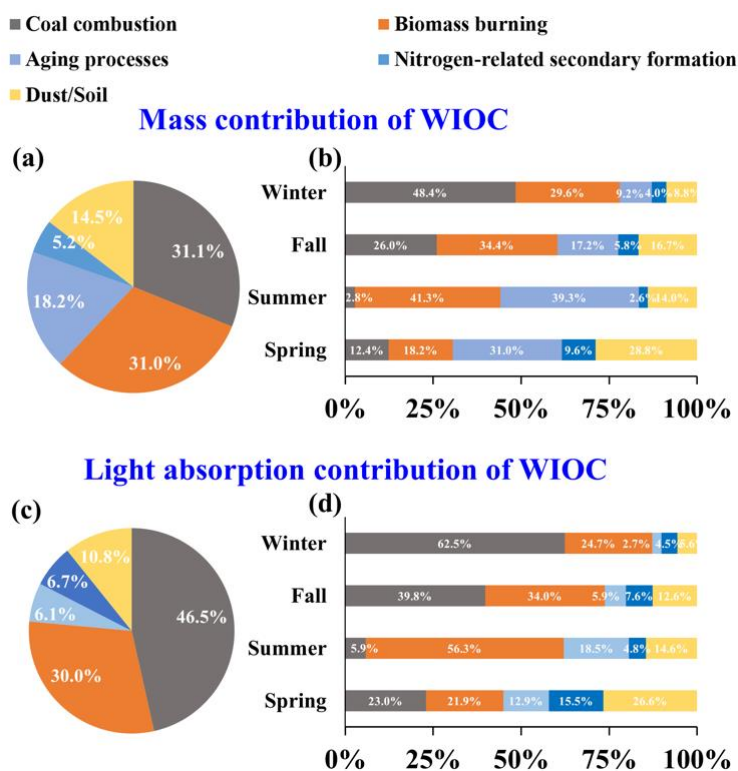
Figure 4. (a) Annual and (b) seasonal sources apportionments result of WIOC mass concentration. (c) Annual and (d) seasonal sources apportionments of WIOC light absorption at 365 nm.

3.3 Radiative forcing of WIOC

The potential radiative of WIOC was estimated by a "simple forcing efficiency" (SFE) method, as described in section 2.5 (Bond and Bergstrom, 2006; Chylek and Wong, 1995). The wavelength-dependent absorption SFE from 300 to 700 nm for WIOC, HULIS and non-HULIS are shown in Figure 5a. The integrated mean SFE from 300 to 700 nm ($SFE_{300-700}$) is highest for WIOC (6.57 ± 5.37 W/g), followed by HULIS (4.39 ± 1.79 W/g) and non-HULIS (1.23 ± 1.03 W/g). This order is consistent with the MAE_{365} of these three fractions (Figure 2c). Comparing the SFE values with previous reports in Chinese cities, the values for WIOC and HULIS fall within the reported range (Hong Kong: 4.40 W/g, Tianjin: 6.30 ± 2.30 W/g, Xi'an: 3.51 ± 2.36 W/g, all for WSOC)(Deng et al., 2022; Li et al., 2023; Zhang et al., 2020a) , but lower than that in Kanpur, India (19.2 W/g, for WSOC) (Choudhary et al., 2021). It is important to note that the SFE values presented here are calculated from bulk light absorbance measurements of the extracts, which tend to be lower than corresponding values from filter-based optical transmission measurements (Li et al., 2020).

468   The radiative effect of light-absorbing OC is generally related to its atmospheric concentration. In

469   equation (8), the concentrations of WIOC, HULIS, and non-HULIS were further taken into account and

470   used to estimate their relative contributions to the solar radiation absorbed by EX-OC (Figure 5b). The

471   fraction of radiative forcing by WIOC ($39.4 \pm 15.5\%$) was almost equal to that of HULIS ($39.5 \pm 12.1\%$),

472   but much higher than non-HULIS ($21.1 \pm 10.2\%$). This result suggests that the radiative forcing of EX-OC

473   is dominantly contributed by the relatively hydrophobic OC fractions, making them efficient radiative-

474   forcing agents. In contrast, consistent with previous studies, the radiative effects of oxidized OC fractions

475   are relatively limited (Tian et al., 2023). Overall, the radiative forcing of different components of OC is

476   highly inhomogeneous, likely associated with their sources and atmospheric processes.

477

478
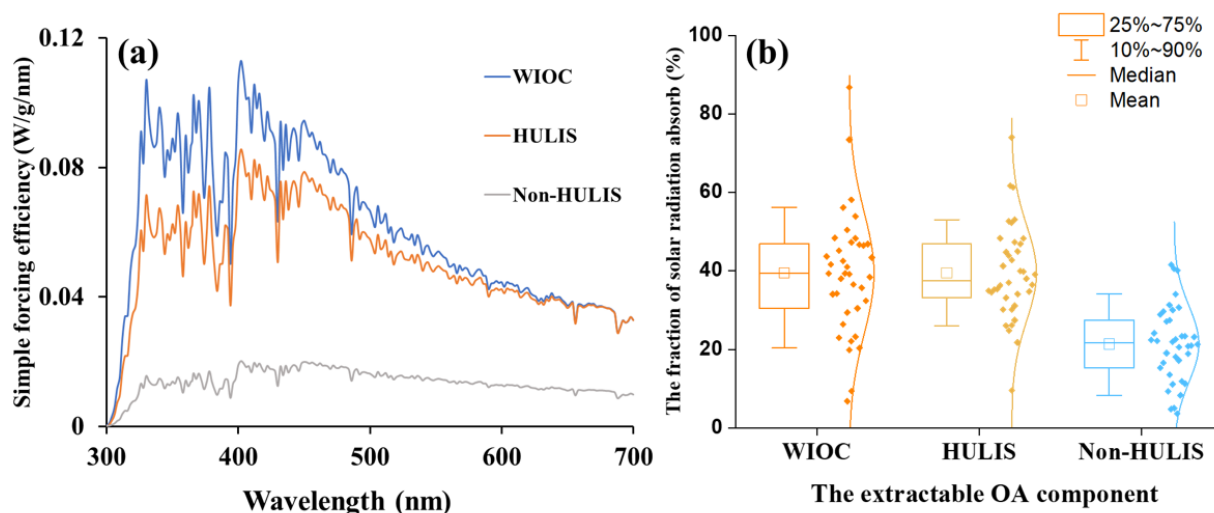
479

480 **Figure 5.** (a) The average simple forcing efficiency (SFE) of the WIOC, HULIS and WSOC from 300 to

481 700 nm; (b) The fraction of solar radiation absorbed by WIOC, HULIS and non-HULIS relative to total

482 extractable OC. The relative fraction of non-HULIS is calculated by the difference between WSOC and

483 HULIS.

484

485

3.4 Possible continuum of light-absorbing carbonaceous components: aromaticity,

486

sources, and atmospheric processes

487

488   The light-absorbing carbonaceous aerosols has conventionally been classified into BC and BrC.

489 Following the classification framework introduced by Saleh (2020), we mapped the BC and BrC in an

490 AAE-logMAE$_{405}$ space. Within the space, BrC can be further categorized into the following: very weakly

(VW), weakly (W), moderately (M), and strongly (S) light-absorbing BrC. In this framework, hydrophobic OC, represented by WIOC and HULIS, falls into the M-BrC area. On the other hand, the relatively hydrophilic OC (e.g., non-HULIS) is skewed more toward the W-BrC area (Figure 6a). It is important to note that WIOC in this study refers to OC that is insoluble in water but soluble in methanol. Thus, WIOC, HULIS, and non-HULIS are considered as extractable OC, implying that all solvent-extractable OC falls within the W- and M-BrC categories. It should be emphasized that S/Dark-BrC, characterized by light-absorbing properties similar to BC, is typically unextractable, as demonstrated in previous studies (Chakrabarty et al., 2023; Corbin et al., 2019). Similarly, BC is traditionally considered unextractable and exhibits the strongest light-absorbing capacity among the various carbonaceous components. According to the chemical and physical properties, BC can be further subdivided into soot-BC and char-BC (Han et al., 2010; Masiello, 2004). Char and soot are defined differently across various environmental matrices (Coppola et al., 2022). For the carbonaceous aerosols, the char-BC and soot-BC are widely and operationally defined by different temperatures in the Interagency Monitoring of Protected Visual Environments (IMPROVE) protocol and the thermal-optical reflectance (TOR) method for OC and EC analysis (Cai et al., 2023; Han et al., 2010). Generally, the light-absorbing capacity of soot-BC is higher than char-BC (Andreae and Gelencser, 2006; Corbin et al., 2019; Schnaiter et al., 2003). The gradual enhancement of the light-absorbing capacity within the carbonaceous components is intricately linked to their molecular structure, specific sources, and atmospheric processes.
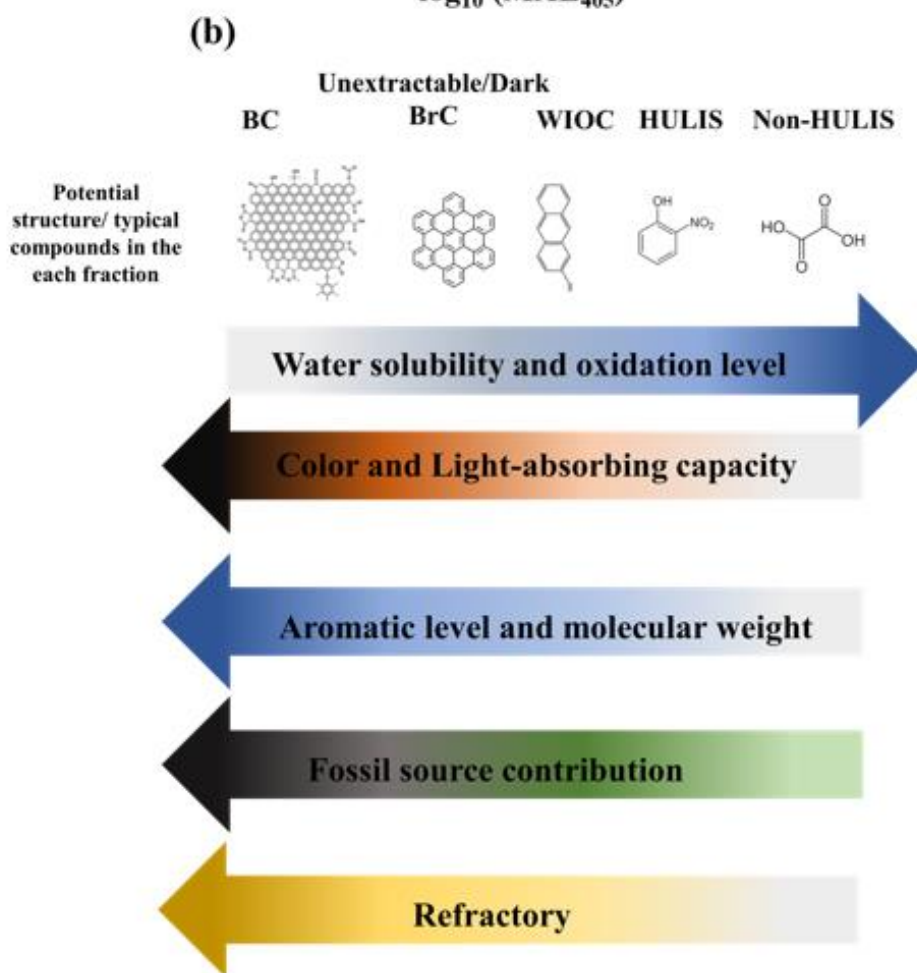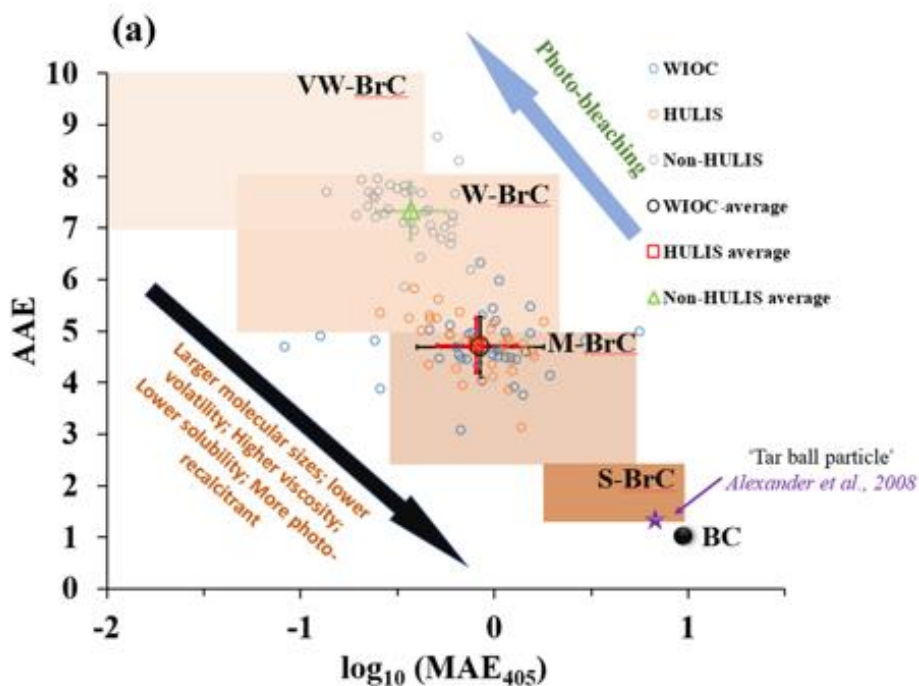
Figure 6. (a) The light-absorbing properties of WIOC, HULIS and Non-HULIS mapped in the in the $\log_{10}(MAE_{405\ nm})$ – AAE space following the approach of Saleh (2020). Brown-shaded areas indicate "very weakly (VW)", "weakly (W)", "moderately (M)", and "strongly (S)" light-absorbing BrC classes. The star symbol marks the upper limit of individual "tar ball particles" inferred from the electron energy loss Spectro

microscopy (Alexander et al., 2008).The AAE is calculated for the wavelength range 330 to 400 nm in this study. (b) The continuum of light-absorbing capacity, water solubility, aromaticity, source and refractory of different carbonaceous components. Arrows indicate the direction of increase. The WIOC in this study does not strictly denote OC that is insoluble in water, it is more likely to be OC that is insoluble in water but soluble in methanol.

In Figure 6b, we proposed a possible light-absorbing continuum of carbonaceous aerosols. The light-absorbing properties of carbonaceous aerosols are largely dependent on their molecular structure, the aromatic molecules have been shown to be the most important fractions relevant to the light-absorbing properties (Andreae and Gelencser, 2006; Bond et al., 2013; Laskin et al., 2015). Generally, the light-absorbing capacity increased with the aromatic level/fractions. For instance, most of BC and dark-BrC as the unextractable and strong light-absorbing components, are enriched with carbon-rich aromatic molecules (Corbin et al., 2019; El Hajj et al., 2021; Saleh, 2020). BC is composed of large polycyclic aromatics with graphitic-like structures (Pöschl, 2005). According to the chemical and physical properties, BC can be further subdivided into soot-BC and char-BC (Han et al., 2010; Masiello, 2004). Due to higher the sp^2-bond carbon and aromatic level of soot-BC, the light-absorbing capacity of soot-BC is higher than char-BC (Andreae and Gelencser, 2006; Corbin et al., 2019; Schnaiter et al., 2003). Dark-BrC, also known as tar balls, is also unextractable light-absorbing carbonaceous component, which exhibits light-absorbing properties similar to BC. The dark-BrC could be considered as incipient BC, characterized by lower molecular weight and aromatic levels compared to mature BC (El Hajj et al., 2021; Saleh et al., 2018). For the extractable hydrophobic OC fraction (e.g., WIOC and HULIS), the aromatic compounds, including PAHs, nitrophenol, and O-/N-aromatics, are the major light-absorbing components (Laskin et al., 2015). Notably, both the molecular weight and aromatic level of aromatic compounds in the extractable hydrophobic OC fraction are commonly lower than those in dark-BrC (Chakrabarty et al., 2023; Corbin et al., 2019). Thus, both the WIOC and HULIS located in the M-BrC space as shown in the Figure 6a. In this study, optical parameters (E2/E3 and AAE) do not reveal a significant difference in molecular weight and aromatic levels between HULIS and WIOC. This discrepancy may be attributed to the limited reliability and accuracy of these optical parameters in reflecting molecular weight and aromaticity. However, employing robust analytical technologies, such as ultra-resolution mass spectrometry and benzene-poly-carboxylic acids tracers (Sun et al., 2021; Tang et al., 2020), studies has demonstrated higher aromatic fraction and aromaticity for WIOC compared to HULIS (Huang et al., 2020; Sun et al., 2021; Tang et al.,

2020). Particularly, polycyclic aromatics are identified as key fractions determining both the light absorptivity and wavelength dependence of WIOC from biomass burning source samples (Sun et al., 2021). Compared with hydrophobic OC, the hydrophilic OC exhibits much lower molecular weight and aromaticity. This is evidenced by the much lower E2/E3 and AAE values of hydrophobic OC than the hydrophilic OC (Figures 3b and c). Overall, the light-absorbing capacity (or color) of carbonaceous components follows the order: soot-BC > char-BC > dark-BrC > WIOC > HULIS > non-HULIS. The light-absorbing capacity and molecular weight of carbonaceous components increase with their aromaticity, while water solubility/polarity decreases with increasing aromaticity.

The molecular structure of carbonaceous components is highly related to specific sources. The BC as carbonaceous with highest aromatic level, is exclusively emitted from incomplete combustion of BB and fossil fuel (Bond et al., 2013). The content of soot-/char-BC from distinct primary emission sources significantly varies with fuel type and combustion conditions (Cai et al., 2023; Han et al., 2021). Soot-BC, formed in high-temperature combustion conditions and with high aromatic contents in the fuel, is more prevalent in fossil fuel combustion processes (e.g., coal and gasoline) than in BB (Han et al., 2021; El Hajj et al., 2021). Thus, soot-BC is predominantly contributed by fossil fuel combustion, while char-BC is the dominant subgroup in BB (Cai et al., 2023; Han et al., 2010). Remarkably, despite the subgroup distinctions within BC, as the strongest light-absorbing carbonaceous component, over 70% of BC in the ambient aerosols from major city clusters in China is attributed to fossil fuel combustion (Jiang et al., 2020a). Regarding the BrC, in addition to sharing primary emission sources with BC, it can also be formed secondarily through complex chemical reactions (Laskin et al., 2015). Dark-BrC as strongest light-absorbing OC, predominantly derived from incomplete combustion of BB and fossil fuels. Laboratory experiments and field observations consistently show that dark-BrC is more abundant in BB plumes (Chakrabarty et al., 2023; Mathai et al., 2023). However, it is noteworthy that controlled-combustion experiments report fossil fuel-derived dark-BrC may exhibit a stronger light-absorbing capacity than BB-derived dark-BrC (Cheng et al., 2019; Yu et al., 2021). Concerning the WIOC, our PMF-based sources apportionment results cannot distinctly differentiate between fossil and non-fossil sources for WIOC. However, radiocarbon isotope ($\Delta^{14}C$), a more robust source apportionment method, has demonstrated that, despite variations in sampling locations and seasons, fossil sources are more enriched in WIOC than WSOC in ambient aerosols from South/East Asia and the U.S.A. (Dasari et al., 2019; Kirillova et al., 2014; Wozniak et al., 2012; Kirillova et al., 2013). In the water-soluble fractions, the HULIS as relatively hydrophobic

WSOC, our previous study using radiocarbon isotope (Δ^{14}C) have shown that the HULIS across ten Chinese cities exhibit a higher fossil contribution than hydrophilic WSOC (e.g., non-HULIS) (48.9 ± 9.0 % vs. 30.3 ± 13.9 %, $p < 0.01$) (Mo et al., 2024). By correlating the light-absorbing capacity with the variation in the sources of different carbonaceous components, as discussed above, we observe that more strongly absorbing carbonaceous components tend to be more enriched with fossil sources.

Upon emission or generation into the atmosphere, the light-absorbing properties of carbonaceous aerosols undergo dynamic changes significantly influenced by atmospheric processes (Dasari et al., 2019; Laskin et al., 2015). The response of different carbonaceous components to atmospheric processes varies extensively. The BC is refractory carbonaceous component in the aerosols, which is recalcitrant to the chemical oxidation. Although laboratory studies reported that the BC is possible oxidized and release water-soluble component under specific conditions (Decesari et al., 2002). But BC is often cored with OC in the ambient aerosols, making somewhat shielded towards oxidants (Bond et al., 2013). Similarly, dark-BrC exhibits considerable resistance to sunlight-driven photochemical bleaching, resulting in the persistence of light-absorbing organic aerosols in the atmosphere (Chakrabarty et al., 2023). This resistance is likely associated with the high viscosity of dark-BrC, limiting surface and bulk reaction rates. Consequently, unextractable light-absorbing components (BC + dark-BrC) not only display strong light absorptivity but also persist longer in the atmosphere. For the WIOC, based on the PMF model results, we found that the WIOC was enriched with primary emissions sources (e.g., coal combustion and BB) than WSOC. This indicated the WIOC is more recalcitrant than WSOC. Indeed, employing dual carbon isotopes (δ^{13}C- Δ^{14}C), studies found that WIOC is not only enriched with fossil sources, but also exhibit greater persistence and relatively longer lifetimes compared to WSOC components present in ambient aerosols (Kirillova et al., 2014; Kirillova et al., 2013; Wozniak et al., 2012). Similar to WIOC, fossil components in HULIS are more resistant and less susceptible to oxidative photobleaching, contributing to their relatively high light-absorbing capacity compared to non-HULIS components (Mo et al., 2024). Generally, chromophores in the aqueous phase experience rapid photo-bleaching, while those in the viscous organic phase undergo slower rates of photo-degradation (Klodt et al., 2022). The recalcitrant properties of WIOC and HULIS may stem from the tendency of these hydrophobic OC components to partition into the viscous organic phase, potentially rendering them more photo-recalcitrant. By linking the light-absorbing capacity to the refractory of different carbonaceous component as discussed above, the strongly light-absorbing carbonaceous

607 components tend to be more recalcitrant in the atmospheres (Figure 6b).

608

609 It is important to acknowledge that carbonaceous aerosols encompass a wide array of diverse
610 components, exhibiting a continuum of physical and chemical properties. The distinction between these
611 carbonaceous components, as discussed above, is primarily based on conceptual and operational definitions,
612 rather than clear boundaries in reality. In other words, the classification of carbonaceous components in
613 aerosols is highly dependent on operational criteria. In this study, on the one hand, the WIOC, HULIS-C,
614 and non-HULIS-C are well-defined based on their polarity. On the other hand, the definition of BC, which
615 includes char- and soot-BC, is more closely associated with thermal and optical properties. These
616 operational definitions may lead to overlaps between different carbonaceous components. For instance. BB
617 and coal combustion emit large amounts of large molecular weight soluble compounds, such as HULIS
618 (e.g., HULIS), which may char and produce false char EC signals in the TOT analysis (Yu et al., 2002).
619 Additionally, certain portions of char-BC may exhibit chemical and physical behaviors akin to high-
620 molecular-weight OC compounds, thereby overlapping with BrC. Therefore, there is no a clear boundary
621 for the carbonaceous components.

622

623 Taken together, we propose a continuum for light-absorbing carbonaceous aerosols, taking into account
624 factors such as aromaticity, molecular weight, sources, polarity and atmospheric processes (Figures 6a and
625 b). The light-absorbing capacity of carbonaceous components exibit following orders: soot-BC > char-
626 BC > dark-BrC > WIOC > HULIS > non-HULIS. This hierarchy indicates that the light-absorbing capacity
627 of carbonaceous components increases with aromaticity, molecular weight, fossil sources contribution, and
628 refractoriness. Conversely, as the polarity/oxidized level of carbonaceous components increases, their light
629 absorbing-capacity weakens. These findings suggest that fossil fuel combustion tends to generate relatively
630 long-term and strongly light-absorbing carbonaceous components. In contrast, light-absorbing
631 carbonaceous components derived from biomass burning are prone to photo-degradation, transforming into
632 colorless carbon with high polarity and cloud condensation activity.

633

634

4. Conclusions

636 In this study, we investigated the light-absorbing properties and sources of WIOC in ten representative

urban cities across China. We found that WIOC averagely accounts for a substantial portion of the concentrations ($33.4 \pm 7.66\%$) and Abs_{365} ($40.5 \pm 9.73\%$) of extractable OC (EX-OC). The MAE_{365} of WIOC (1.59 ± 0.55 m^2/gC) was comparable to that of HULIS (1.54 ± 0.57 m^2/gC) but significantly higher than non-HULIS (0.71 ± 0.28 m^2/gC), suggesting the stronger light-absorbing capacity of hydrophobic OC (WIOC+HULIS) compared to hydrophilic OC (non-HULIS). The dominant sources of WIOC were biomass burning (31.0%) and coal combustion (31.1%), with coal combustion exhibiting the highest light-absorbing capacity among these sources. Moreover, utilizing the simple forcing efficiency ($SFE_{300-700nm}$) method, we found that WIOC exhibited the highest $SFE_{300-700nm}$ (6.57 ± 5.37 W/g) among the EX-OC fractions. Notably, the radiative forcing of EX-OC was predominantly attributed to hydrophobic OC (WIOC: $39.4 \pm 15.5\%$ and HULIS: $39.5 \pm 12.1\%$). Finally, we proposed a light-absorbing carbonaceous continuum based on considerations of aromaticity, sources, and atmospheric processes of different carbonaceous components. This continuum revealed that carbonaceous components more enriched with fossil sources tend to possess stronger light-absorbing capacity, higher aromatic levels, increased molecular weights, and greater recalcitrance in the atmosphere. The implications of our study underscore the necessity of reducing fossil fuel emissions as an effective strategy for mitigating both gaseous (CO_2) and particulate light-absorbing carbonaceous warming components.

Author Contributions

Conceptualization: Yangzhi Mo; **Funding acquisition:** Gan Zhang; **Investigation:** Yangzhi Mo, Jiao Tang, Hongxing Jiang, Zhineng Cheng, Sanyuan Zhu; **Methodology:** Yangzhi Mo; **Project Administration:** Gan Zhang, Shizhen Zhao; **Resources:** Sanyuan Zhu, Yingjun Chen, Chongguo Tian, Zhineng Cheng, Gan Zhang; **Software:** Yangzhi Mo; **Supervision:** Guangcai Zhong, Jun Li,Gan Zhang; **Validation:** Yangzhi Mo, Jun Li; **Writing – original draft:** Yangzhi Mo; **Writing – review & editing:** Yangzhi Mo, Jun Li, Gan Zhang

Competing interests

The contact author has declared that none of the authors has any competing interests.

Data availability

The code and data supporting the conclusions of this paper are available upon request.

Acknowledgements

This study was supported by the Natural Science Foundation of China (NSFC; No. 42030715, 42192511, and 42107121), the Alliance of International Science Organizations (Grant No. ANSO-CR-KP-2021-05), the Guangdong Basic and Applied Basic Research Foundation (2021A0505020017, 2023A1515012359 and 2023B1515020067), and a scholarship for Yangzhi Mo provided by the China Scholarship Council (202204910172). The authors gratefully thank the people at all sites for sample collections and all of the individuals and groups participating in this project.

References

Alexander, D. T. L., Crozier, P. A., and Anderson, J. R.: Brown Carbon Spheres in East Asian Outflow and Their Optical Properties, Science, 321, 833-836, https://doi:10.1126/science.1155296, 2008.

Andreae, M. O. and Gelencser, A.: Black carbon or brown carbon? The nature of light-absorbing carbonaceous aerosols, Atmospheric Chemistry and Physics, 6, 3131-3148, https://10.5194/acp-6-3131-2006, 2006.

Arola, A., Schuster, G., Myhre, G., Kazadzis, S., Dey, S., and Tripathi, S. N.: Inferring absorbing organic carbon content from AERONET data, Atmospheric Chemistry and Physics, 11, 215-225, https://10.5194/acp-11-215-2011, 2011.

Baduel, C., Voisin, D., and Jaffrezo, J. L.: Seasonal variations of concentrations and optical properties of water soluble HULIS collected in urban environments, Atmospheric Chemistry and Physics, 10, 4085-4095, https://10.5194/acp-10-4085-2010, 2010.

Bahadur, R., Praveen, P. S., Xu, Y. Y., and Ramanathan, V.: Solar absorption by elemental and brown carbon determined from spectral observations, Proceedings of the National Academy of Sciences of the United States of America, 109, 17366-17371, https://10.1073/pnas.1205910109, 2012.

Bond, T. C.: Spectral dependence of visible light absorption by carbonaceous particles emitted from coal combustion, Geophysical Research Letters, 28, 4075-4078, https://10.1029/2001gl013652, 2001.

Bond, T. C. and Bergstrom, R. W.: Light absorption by carbonaceous particles: An investigative review, Aerosol Science and Technology, 40, 27-67, https://10.1080/02786820500421521, 2006.

Bond, T. C., Doherty, S. J., Fahey, D. W., Forster, P. M., Berntsen, T., DeAngelo, B. J., Flanner, M. G.,

Ghan, S., Kärcher, B., Koch, D., Kinne, S., Kondo, Y., Quinn, P. K., Sarofim, M. C., Schultz, M. G., Schulz, M., Venkataraman, C., Zhang, H., Zhang, S., Bellouin, N., Guttikunda, S. K., Hopke, P. K., Jacobson, M. Z., Kaiser, J. W., Klimont, Z., Lohmann, U., Schwarz, J. P., Shindell, D., Storelvmo, T., Warren, S. G., and Zender, C. S.: Bounding the role of black carbon in the climate system: A scientific assessment, Journal of Geophysical Research-Atmospheres, 118, 5380-5552, https://10.1002/jgrd.50171, 2013.

Bosch, C., Andersson, A., Kirillova, E. N., Budhavant, K., Tiwari, S., Praveen, P. S., Russell, L. M., Beres, N. D., Ramanathan, V., and Gustafsson, O.: Source-diagnostic dual-isotope composition and optical properties of water-soluble organic carbon and elemental carbon in the South Asian outflow intercepted over the Indian Ocean, Journal of Geophysical Research-Atmospheres, 119, 11743-11759, https://10.1002/2014jd022127, 2014.

Cai, J., Jiang, H., Chen, Y., Liu, Z., Han, Y., Shen, H., Song, J., Li, J., Zhang, Y., Wang, R., Chen, J., and Zhang, G.: Char dominates black carbon aerosol emission and its historic reduction in China, Nature Communications, 14, 6444, https://10.1038/s41467-023-42192-8, 2023.

Chakrabarty, R. K., Shetty, N. J., Thind, A. S., Beeler, P., Sumlin, B. J., Zhang, C. C., Liu, P., Idrobo, J. C., Adachi, K., Wagner, N. L., Schwarz, J. P., Ahern, A., Sedlacek, A. J., Lambe, A., Daube, C., Lyu, M., Liu, C., Herndon, S., Onasch, T. B., and Mishra, R.: Shortwave absorption by wildfire smoke dominated by dark brown carbon, Nature Geoscience, 16, https://10.1038/s41561-023-01237-9, 2023.

Chen, Q., Ikemori, F., Nakamura, Y., Vodicka, P., Kawamura, K., and Mochida, M.: Structural and Light-Absorption Characteristics of Complex Water-Insoluble Organic Mixtures in Urban Submicrometer Aerosols, Environ. Sci. Technol., 51, 8293-8303, https://10.1021/acs.est.7b01630, 2017.

Chen, Q. C., Ikemori, F., and Mochida, M.: Light Absorption and Excitation-Emission Fluorescence of Urban Organic Aerosol Components and Their Relationship to Chemical Structure, Environmental Science & Technology, 50, 10859-10868, https://10.1021/acs.est.6b02541, 2016.

Chen, Y. and Bond, T. C.: Light absorption by organic carbon from wood combustion, Atmos. Chem. Phys., 10, 1773-1787, https://10.5194/acp-10-1773-2010, 2010.

Cheng, Y., He, K.-b., Du, Z.-y., Engling, G., Liu, J.-m., Ma, Y.-l., Zheng, M., and Weber, R. J.: The characteristics of brown carbon aerosol during winter in Beijing, Atmos. Environ., 127, 355-364, https://10.1016/j.atmosenv.2015.12.035, 2016.

Cheng, Z. Z., Atwi, K., Onyima, T., and Saleh, R.: Investigating the dependence of light-absorption properties of combustion carbonaceous aerosols on combustion conditions, Aerosol Science and Technology, 53, 419-434, https://10.1080/02786826.2019.1566593, 2019.

Choudhary, V., Rajput, P., and Gupta, T.: Absorption properties and forcing efficiency of light-absorbing water-soluble organic aerosols: Seasonal and spatial variability, Environmental Pollution, 272, https://10.1016/j.envpol.2020.115932, 2021.

Chylek, P. and Wong, J.: EFFECT OF ABSORBING AEROSOLS ON GLOBAL RADIATION BUDGET, Geophysical Research Letters, 22, 929-931, https://10.1029/95gl00800, 1995.

Coppola, A. I., Wagner, S., Lennartz, S. T., Seidel, M., Ward, N. D., Dittmar, T., Santín, C., and Jones, M. W.: The black carbon cycle and its role in the Earth system, Nature Reviews Earth & Environment, 3, 516-532, https://10.1038/s43017-022-00316-6, 2022.

Corbin, J. C., Czech, H., Massabò, D., de Mongeot, F. B., Jakobi, G., Liu, F., Lobo, P., Mennucci, C., Mensah, A. A., Orasche, J., Pieber, S. M., Prévôt, A. S. H., Stengel, B., Tay, L. L., Zanatta, M., Zimmermann, R., El Haddad, I., and Gysel, M.: Infrared-absorbing carbonaceous tar can dominate light absorption by marine-engine exhaust, Npj Climate and Atmospheric Science, 2, https://10.1038/s41612-019-0069-5, 2019.

Dasari, S., Andersson, A., Bikkina, S., Holmstrand, H., Budhavant, K., Satheesh, S., Asmi, E., Kesti, J., Backman, J., Salam, A., Bisht, D. S., Tiwari, S., Hameed, Z., and Gustafsson, O.: Photochemical degradation affects the light absorption of water-soluble brown carbon in the South Asian outflow, Science Advances, 5, https://10.1126/sciadv.aau8066, 2019.

Decesari, S., Facchini, M. C., Matta, E., Mircea, M., Fuzzi, S., Chughtai, A. R., and Smith, D. M.: Water soluble organic compounds formed by oxidation of soot, Atmospheric Environment, 36, 1827-1832, https://10.1016/s1352-2310(02)00141-3, 2002.

Deng, J., Ma, H., Wang, X., Zhong, S., Zhang, Z., Zhu, J., Fan, Y., Hu, W., Wu, L., Li, X., Ren, L., Pavuluri, C. M., Pan, X., Sun, Y., Wang, Z., Kawamura, K., and Fu, P.: Measurement report: Optical properties and sources of water-soluble brown carbon in Tianjin, North China – insights from organic molecular compositions, Atmos. Chem. Phys., 22, 6449-6470, https://10.5194/acp-22-6449-2022, 2022.

Du, Z. Y., He, K. B., Cheng, Y., Duan, F. K., Ma, Y. L., Liu, J. M., Zhang, X. L., Zheng, M., and Weber, R.: A yearlong study of water-soluble organic carbon in Beijing II: Light absorption properties, Atmospheric Environment, 89, 235-241, https://10.1016/j.atmosenv.2014.02.022, 2014.

Duarte, R., Pio, C. A., and Duarte, A. C.: Spectroscopic study of the water-soluble organic matter isolated from atmospheric aerosols collected under different atmospheric conditions, Analytica Chimica Acta, 530, 7-14, https://10.1016/j.aca.2004.08.049, 2005.

El Hajj, O., Atwi, K., Cheng, Z., Koritzke, A. L., Christianson, M. G., Dewey, N. S., Rotavera, B., and

Saleh, R.: Two-stage aerosol formation in low-temperature combustion, Fuel, 304, https://10.1016/j.fuel.2021.121322, 2021.

Fan, X., Song, J., and Peng, P. a.: Comparison of isolation and quantification methods to measure humic-like substances (HULIS) in atmospheric particles, Atmospheric Environment, 60, 366-374, https://10.1016/j.atmosenv.2012.06.063, 2012.

Fan, X., Wei, S., Zhu, M., Song, J., and Peng, P. a.: Comprehensive characterization of humic-like substances in smoke PM2.5 emitted from the combustion of biomass materials and fossil fuels, Atmospheric Chemistry and Physics, 16, 13321-13340, https://10.5194/acp-16-13321-2016, 2016.

Fellman, J. B., Hood, E., Raymond, P. A., Stubbins, A., and Spencer, R. G. M.: Spatial Variation in the Origin of Dissolved Organic Carbon in Snow on the Juneau Icefield, Southeast Alaska, Environmental Science & Technology, 49, 11492-11499, https://10.1021/acs.est.5b02685, 2015.

Feng, Y., Ramanathan, V., and Kotamarthi, V. R.: Brown carbon: a significant atmospheric absorber of solar radiation?, Atmospheric Chemistry and Physics, 13, 8607-8621, https://10.5194/acp-13-8607-2013, 2013.

Filonchyk, M., Peterson, M. P., Zhang, L., and Yan, H.: An analysis of air pollution associated with the 2023 sand and dust storms over China: Aerosol properties and PM10 variability, Geoscience Frontiers, 15, 101762, https://https://doi.org/10.1016/j.gsf.2023.101762, 2024.

Han, L. H., Zhuang, G. S., Cheng, S. Y., Wang, Y., and Li, J.: Characteristics of re-suspended road dust and its impact on the atmospheric environment in Beijing, Atmospheric Environment, 41, 7485-7499, https://10.1016/j.atmosenv.2007.05.044, 2007.

Han, Y., Chen, Y. J., Feng, Y. L., Shang, Y., Li, J., Li, Q., and Chen, J. M.: Fuel Aromaticity Promotes Low-Temperature Nucleation Processes of Elemental Carbon from Biomass and Coal Combustion, Environmental Science & Technology, 55, 2532-2540, https://10.1021/acs.est.0c06694, 2021.

Han, Y. M., Cao, J. J., Lee, S. C., Ho, K. F., and An, Z. S.: Different characteristics of char and soot in the atmosphere and their ratio as an indicator for source identification in Xi'an, China, Atmos. Chem. Phys., 10, 595-607, https://10.5194/acp-10-595-2010, 2010.

Hecobian, A., Zhang, X., Zheng, M., Frank, N., Edgerton, E. S., and Weber, R. J.: Water-Soluble Organic Aerosol material and the light-absorption characteristics of aqueous extracts measured over the Southeastern United States, Atmospheric Chemistry and Physics, 10, 5965-5977, https://10.5194/acp-10-5965-2010, 2010.

Huang, R.-J., Yang, L., Shen, J., Yuan, W., Gong, Y., Guo, J., Cao, W., Duan, J., Ni, H., Zhu, C., Dai, W., Li, Y., Chen, Y., Chen, Q., Wu, Y., Zhang, R., Dusek, U., O'Dowd, C., and Hoffmann, T.: Water-Insoluble

Organics Dominate Brown Carbon in Wintertime Urban Aerosol of China: Chemical Characteristics and Optical Properties, Environmental Science & Technology, 54, 7836-7847, https://10.1021/acs.est.0c01149, 2020.

Jiang, F., Liu, J. W., Huang, Z. J., Zheng, J. Y., and Zhang, G.: Progress of the stable carbon and radiocarbon isotopes of black carbon aerosol, Chinese Science Bulletin-Chinese, 65, 4095-4106, https://10.1360/tb-2020-0355, 2020a.

Jiang, H. X., Li, J., Chen, D. H., Tang, J., Cheng, Z. N., Mo, Y. Z., Su, T., Tian, C. G., Jiang, B., Liao, Y. H., and Zhang, G.: Biomass burning organic aerosols significantly influence the light absorption properties of polarity-dependent organic compounds in the Pearl River Delta Region, China, Environment International, 144, https://10.1016/j.envint.2020.106079, 2020b.

Jimenez, J. L., Canagaratna, M. R., Donahue, N. M., Prevot, A. S. H., Zhang, Q., Kroll, J. H., DeCarlo, P. F., Allan, J. D., Coe, H., Ng, N. L., Aiken, A. C., Docherty, K. S., Ulbrich, I. M., Grieshop, A. P., Robinson, A. L., Duplissy, J., Smith, J. D., Wilson, K. R., Lanz, V. A., Hueglin, C., Sun, Y. L., Tian, J., Laaksonen, A., Raatikainen, T., Rautiainen, J., Vaattovaara, P., Ehn, M., Kulmala, M., Tomlinson, J. M., Collins, D. R., Cubison, M. J., Dunlea, E. J., Huffman, J. A., Onasch, T. B., Alfarra, M. R., Williams, P. I., Bower, K., Kondo, Y., Schneider, J., Drewnick, F., Borrmann, S., Weimer, S., Demerjian, K., Salcedo, D., Cottrell, L., Griffin, R., Takami, A., Miyoshi, T., Hatakeyama, S., Shimono, A., Sun, J. Y., Zhang, Y. M., Dzepina, K., Kimmel, J. R., Sueper, D., Jayne, J. T., Herndon, S. C., Trimborn, A. M., Williams, L. R., Wood, E. C., Middlebrook, A. M., Kolb, C. E., Baltensperger, U., and Worsnop, D. R.: Evolution of Organic Aerosols in the Atmosphere, Science, 326, 1525-1529, https://10.1126/science.1180353, 2009.

Kalberer, M., Sax, M., and Samburova, V.: Molecular size evolution of oligomers in organic aerosols collected in urban atmospheres and generated in a smog chamber, Environmental Science & Technology, 40, 5917-5922, https://10.1021/es0525760, 2006.

Kirchstetter, T. W., Novakov, T., and Hobbs, P. V.: Evidence that the spectral dependence of light absorption by aerosols is affected by organic carbon, Journal of Geophysical Research-Atmospheres, 109, https://10.1029/2004jd004999, 2004.

Kirillova, E. N., Andersson, A., Han, J., Lee, M., and Gustafsson, O.: Sources and light absorption of water-soluble organic carbon aerosols in the outflow from northern China, Atmospheric Chemistry and Physics, 14, 1413-1422, https://10.5194/acp-14-1413-2014, 2014.

Kirillova, E. N., Andersson, A., Sheesley, R. J., Kruså, M., Praveen, P. S., Budhavant, K., Safai, P. D., Rao, P. S. P., and Gustafsson, Ö.: [13]C- and ^{14}C-based study of sources and atmospheric processing of water-

soluble organic carbon (WSOC) in South Asian aerosols: 13C AND 14C IN WSOC OF S ASIAN AEROSOLS, Journal of Geophysical Research: Atmospheres, 118, 614-626, https://10.1002/jgrd.50130, 2013.

Kiss, G., Varga, B., Galambos, I., and Ganszky, I.: Characterization of water-soluble organic matter isolated from atmospheric fine aerosol, Journal of Geophysical Research-Atmospheres, 107, https://10.1029/2001jd000603, 2002.

Klodt, A. L., Adamek, M., Dibley, M., Nizkorodov, S. A., and O'Brien, R. E.: Effects of the sample matrix on the photobleaching and photodegradation of toluene-derived secondary organic aerosol compounds, Atmospheric Chemistry and Physics, 22, 10155-10171, https://10.5194/acp-22-10155-2022, 2022.

Laskin, A., Laskin, J., and Nizkorodov, S. A.: Chemistry of Atmospheric Brown Carbon, Chemical Reviews, 115, 4335-4382, https://10.1021/cr5006167, 2015.

Li, X. F., Yu, F., Song, Y. Y., Zhang, C., Yan, F. P., Hu, Z. F., Lei, Y. L., Tripathee, L., Zhang, R., Guo, J. N., Wang, Y. Q., Chen, Q. C., Liu, L., Cao, J. J., and Wang, Q. Y.: Water-soluble brown carbon in PM2.5 at two typical sites in Guanzhong Basin: Optical properties, sources, and implications, Atmospheric Research, 281, https://10.1016/j.atmosres.2022.106499, 2023.

Li, X. H., Xiao, M. D., Xu, X. Z., Zhou, J. C., Yang, K. Q., Wang, Z. H., Zhang, W. J., Hopke, P. K., and Zhao, W. X.: Light Absorption Properties of Organic Aerosol from Wood Pyrolysis: Measurement Method Comparison and Radiative Implications, Environmental Science & Technology, 54, 7156-7164, https://10.1021/acs.est.0c01475, 2020.

Lin, P., Engling, G., and Yu, J. Z.: Humic-like substances in fresh emissions of rice straw burning and in ambient aerosols in the Pearl River Delta Region, China, Atmospheric Chemistry and Physics, 10, 6487-6500, https://10.5194/acp-10-6487-2010, 2010a.

Lin, P., Huang, X.-F., He, L.-Y., and Yu, J. Z.: Abundance and size distribution of HULIS in ambient aerosols at a rural site in South China, J. Aerosol Sci., 41, 74-87, https://10.1016/j.jaerosci.2009.09.001, 2010b.

Lin, P., Fleming, L. T., Nizkorodov, S. A., Laskin, J., and Laskin, A.: Comprehensive Molecular Characterization of Atmospheric Brown Carbon by High Resolution Mass Spectrometry with Electrospray and Atmospheric Pressure Photoionization, Analytical Chemistry, 90, 12493-12502, https://10.1021/acs.analchem.8b02177, 2018.

Liu, J., Bergin, M., Guo, H., King, L., Kotra, N., Edgerton, E., and Weber, R. J.: Size-resolved measurements of brown carbon in water and methanol extracts and estimates of their contribution to

ambient fine-particle light absorption, Atmospheric Chemistry and Physics, 13, 12389-12404, https://10.5194/acp-13-12389-2013, 2013.

Masiello, C. A.: New directions in black carbon organic geochemistry, Marine Chemistry, 92, 201-213, https://10.1016/j.marchem.2004.06.043, 2004.

Mathai, S., Veghte, D., Kovarik, L., Mazzoleni, C., Tseng, K. P., Bucci, S., Capek, T., Cheng, Z. Z., Marinoni, A., and China, S.: Optical Properties of Individual Tar Balls in the Free Troposphere, Environmental Science & Technology, 57, 16834-16842, https://10.1021/acs.est.3c03498, 2023.

Mo, Y., Li, J., Cheng, Z., Zhong, G., Zhu, S., Tian, C., Chen, Y., and Zhang, G.: Dual Carbon Isotope-Based Source Apportionment and Light Absorption Properties of Water-Soluble Organic Carbon in PM2.5 Over China, Journal of Geophysical Research-Atmospheres, 126, https://10.1029/2020jd033920, 2021.

Mo, Y., Li, J., Liu, J., Zhong, G., Cheng, Z., Tian, C., Chen, Y., and Zhang, G.: The influence of solvent and pH on determination of the light absorption properties of water-soluble brown carbon, Atmospheric Environment, 161, 90-98, https://10.1016/j.atmosenv.2017.04.037, 2017.

Mo, Y., Li, J., Zhong, G., Zhu, S., Cheng, Z., Tang, J., Jiang, H., Jiang, B., Liao, Y., Song, J., Tian, C., Chen, Y., Zhao, S., and Zhang, G.: The sources and atmospheric processes of strong light-absorbing components in water soluble brown carbon: Insights from a multi-proxy study of PM2.5 in 10 Chinese cities, Journal of Geophysical Research: Atmospheres, 129, https://doi.org/10.1029/2023JD039512, 2024.

Paterson, K. G.: Analysis of air quality data using positive matrix factorization (vol 33, pg 635, 1999), Environmental Science & Technology, 33, 3283-3283, https://10.1021/es992017r, 1999.

Peuravuori, J. and Pihlaja, K.: Molecular size distribution and spectroscopic properties of aquatic humic substances, Analytica Chimica Acta, 337, 133-149, https://10.1016/s0003-2670(96)00412-6, 1997.

Phillips, S. M., Bellcross, A. D., and Smith, G. D.: Light Absorption by Brown Carbon in the Southeastern United States is pH-dependent, Environmental Science & Technology, 51, 6782-6790, https://10.1021/acs.est.7b01116, 2017.

Pöschl, U.: Atmospheric aerosols:: Composition, transformation, climate and health effects, Angewandte Chemie-International Edition, 44, 7520-7540, https://10.1002/anie.200501122, 2005.

Saleh, R.: From Measurements to Models: Toward Accurate Representation of Brown Carbon in Climate Calculations, Current Pollution Reports, 6, 90-104, https://10.1007/s40726-020-00139-3, 2020.

Saleh, R., Cheng, Z., and Atwi, K.: The Brown-Black Continuum of Light-Absorbing Combustion Aerosols, Environmental Science & Technology Letters, 5, 508-513, https://10.1021/acs.estlett.8b00305, 2018.

Saleh, R., Marks, M., Heo, J., Adams, P. J., Donahue, N. M., and Robinson, A. L.: Contribution of brown

carbon and lensing to the direct radiative effect of carbonaceous aerosols from biomass and biofuel burning emissions, Journal of Geophysical Research-Atmospheres, 120, 10285-10296, https://10.1002/2015jd023697, 2015.

Saleh, R., Hennigan, C. J., McMeeking, G. R., Chuang, W. K., Robinson, E. S., Coe, H., Donahue, N. M., and Robinson, A. L.: Absorptivity of brown carbon in fresh and photo-chemically aged biomass-burning emissions, Atmospheric Chemistry and Physics, 13, 7683-7693, https://10.5194/acp-13-7683-2013, 2013.

Samburova, V., Didenko, T., Kunenkov, E., Emmenegger, C., Zenobi, R., and Kalberer, M.: Functional group analysis of high-molecular weight compounds in the water-soluble fraction of organic aerosols, Atmospheric Environment, 41, 4703-4710, https://10.1016/j.atmosenv.2007.03.033, 2007.

Schnaiter, M., Horvath, H., Möhler, O., Naumann, K. H., Saathoff, H., and Schöck, O. W.: UV-VIS-NIR spectral optical properties of soot and soot-containing aerosols, Journal of Aerosol Science, 34, 1421-1444, https://10.1016/s0021-8502(03)00361-6, 2003.

Song, J., Li, M., Fan, X., Zou, C., Zhu, M., Jiang, B., Yu, Z., Jia, W., Liao, Y., and Peng, P. a.: Molecular Characterization of Water- and Methanol-Soluble Organic Compounds Emitted from Residential Coal Combustion Using Ultrahigh-Resolution Electrospray Ionization Fourier Transform Ion Cyclotron Resonance Mass Spectrometry, Environmental Science & Technology, 53, 13607-13617, https://10.1021/acs.est.9b04331, 2019.

Sun, H. L., Biedermann, L., and Bond, T. C.: Color of brown carbon: A model for ultraviolet and visible light absorption by organic carbon aerosol, Geophysical Research Letters, 34, https://10.1029/2007gl029797, 2007.

Sun, Y., Tang, J., Mo, Y., Geng, X., Zhong, G., Yi, X., Yan, C., Li, J., and Zhang, G.: Polycyclic Aromatic Carbon: A Key Fraction Determining the Light Absorption Properties of Methanol-Soluble Brown Carbon of Open Biomass Burning Aerosols, Environmental Science & Technology, 55, 15724-15733, https://10.1021/acs.est.1c06460, 2021.

Tang, J., Li, J., Su, T., Han, Y., Mo, Y., Jiang, H., Cui, M., Jiang, B., Chen, Y., Tang, J., Song, J., Peng, P. a., and Zhang, G.: Molecular compositions and optical properties of dissolved brown carbon in biomass burning, coal combustion, and vehicle emission aerosols illuminated by excitation-emission matrix spectroscopy and Fourier transform ion cyclotron resonance mass spectrometry analysis, Atmospheric Chemistry and Physics, 20, 2513-2532, https://10.5194/acp-20-2513-2020, 2020.

Tian, J., Wang, Q. Y., Ma, Y. Y., Wang, J., Han, Y. M., and Cao, J. J.: Impacts of biomass burning and photochemical processing on the lightabsorption of brown carbon in the southeastern Tibetan Plateau,

Atmospheric Chemistry and Physics, 23, 1879-1892, https://10.5194/acp-23-1879-2023, 2023.

Verma, V., Rico-Martinez, R., Kotra, N., King, L., Liu, J. M., Snell, T. W., and Weber, R. J.: Contribution of Water-Soluble and Insoluble Components and Their Hydrophobic/Hydrophilic Subfractions to the Reactive Oxygen Species-Generating Potential of Fine Ambient Aerosols, Environmental Science & Technology, 46, 11384-11392, https://10.1021/es302484r, 2012.

Wang, D. W., Yang, X. T., Lu, H. W., Li, D., Xu, H. M., Luo, Y., Sun, J., Ho, S. S. H., and Shen, Z. X.: Oxidative potential of atmospheric brown carbon in six Chinese megacities: Seasonal variation and source apportionment, Atmospheric Environment, 309, https://10.1016/j.atmosenv.2023.119909, 2023.

Wang, Y. Q., Wang, M. M., Li, S. P., Sun, H. Y., Mu, Z., Zhang, L. X., Li, Y. G., and Chen, Q. C.: Study on the oxidation potential of the water-soluble components of ambient PM2.5 over Xi'an, China: Pollution levels, source apportionment and transport pathways, Environment International, 136, https://10.1016/j.envint.2020.105515, 2020.

Wong, J. P. S., Nenes, A., and Weber, R. J.: Changes in Light Absorptivity of Molecular Weight Separated Brown Carbon Due to Photolytic Aging, Environmental Science & Technology, 51, 8414-8421, https://10.1021/acs.est.7b01739, 2017.

Wozniak, A. S., Willoughby, A. S., Gurganus, S. C., and Hatcher, P. G.: Distinguishing molecular characteristics of aerosol water soluble organic matter from the 2011 trans-North Atlantic US GEOTRACES cruise, Atmospheric Chemistry and Physics, 14, 8419-8434, https://10.5194/acp-14-8419-2014, 2014.

Wozniak, A. S., Bauer, J. E., Dickhut, R. M., Xu, L., and McNichol, A. P.: Isotopic characterization of aerosol organic carbon components over the eastern United States, Journal of Geophysical Research-Atmospheres, 117, https://10.1029/2011jd017153, 2012.

Xie, M., Chen, X., Hays, M. D., Lewandowski, M., Offenberg, J., Kleindienst, T. E., and Holder, A. L.: Light Absorption of Secondary Organic Aerosol: Composition and Contribution of Nitroaromatic Compounds, Environmental Science & Technology, 51, 11607-11616, https://10.1021/acs.est.7b03263, 2017.

Yan, C., Zheng, M., Bosch, C., Andersson, A., Desyaterik, Y., Sullivan, A. P., Collett, J. L., Zhao, B., Wang, S., He, K., and Gustafsson, O.: Important fossil source contribution to brown carbon in Beijing during winter, Scientific Reports, 7, https://10.1038/srep43182, 2017.

Yu, J. Z., Xu, J., and Yang, H.: Charring Characteristics of Atmospheric Organic Particulate Matter in Thermal Analysis, Environmental Science & Technology, 36, 754-761, https://10.1021/es015540q, 2002.

Yu, Z. H., Cheng, Z. Z., Magoon, G. R., El Hajj, O., and Saleh, R.: Characterization of light-absorbing aerosols from a laboratory combustion source with two different photoacoustic techniques, Aerosol Science and Technology, 55, 387-397, https://10.1080/02786826.2020.1849537, 2021.

Zhang, Q., Shen, Z., Zhang, L., Zeng, Y., Ning, Z., Zhang, T., Lei, Y., Wang, Q., Li, G., Sun, J., Westerdahl, D., Xu, H., and Cao, J.: Investigation of Primary and Secondary Particulate Brown Carbon in Two Chinese Cities of Xi'an and Hong Kong in Wintertime, Environmental Science & Technology, 54, 3803-3813, https://10.1021/acs.est.9b05332, 2020a.

Zhang, Q., Jimenez, J. L., Canagaratna, M. R., Allan, J. D., Coe, H., Ulbrich, I., Alfarra, M. R., Takami, A., Middlebrook, A. M., Sun, Y. L., Dzepina, K., Dunlea, E., Docherty, K., DeCarlo, P. F., Salcedo, D., Onasch, T., Jayne, J. T., Miyoshi, T., Shimono, A., Hatakeyama, S., Takegawa, N., Kondo, Y., Schneider, J., Drewnick, F., Borrmann, S., Weimer, S., Demerjian, K., Williams, P., Bower, K., Bahreini, R., Cottrell, L., Griffin, R. J., Rautiainen, J., Sun, J. Y., Zhang, Y. M., and Worsnop, D. R.: Ubiquity and dominance of oxygenated species in organic aerosols in anthropogenically-influenced Northern Hemisphere midlatitudes, Geophysical Research Letters, 34, https://10.1029/2007gl029979, 2007.

Zhang, T., Shen, Z. X., Zhang, L. M., Tang, Z. Y., Zhang, Q., Chen, Q. C., Lei, Y. L., Zeng, Y. L., Xu, H. M., and Cao, J. J.: PM$_{2.5}$ Humic-like substances over Xi'an, China: Optical properties, chemical functional group, and source identification, Atmospheric Research, 234, https://10.1016/j.atmosres.2019.104784, 2020b.

Zhang, X. L., Lin, Y. H., Surratt, J. D., and Weber, R. J.: Sources, Composition and Absorption Angstrom Exponent of Light-absorbing Organic Components in Aerosol Extracts from the Los Angeles Basin, Environmental Science & Technology, 47, 3685-3693, https://10.1021/es305047b, 2013.

Zhang, Y., Ma, Y., and Gong, W.: Retrieval of Brown Carbon based on the aerosol complex refractive indices in the winter of Wuhan, Geo-spatial Information Science, 20, 319-324, https://10.1080/10095020.2017.1394660, 2017.